Geochemistry, Geophysics, Geosystems®

RESEARCH ARTICLE
10.1029/2023GC011273

Depth-Partitioning of Particulate Organic Carbon Composition in the Rising and Falling Stages of the Amazon River

Sarah Z. Rosengard[1,2,3], Jose Mauro S. Moura[4], Robert G. M. Spencer[5], Carl Johnson[1], Ann McNichol[6], Andrew D. Steen[7], and Valier Galy[1]

[1]Department of Marine Chemistry and Geochemistry, Woods Hole Oceanographic Institution, Woods Hole, MA, USA, [2]Department of Earth, Atmospheric and Planetary Sciences, Massachusetts Institute of Technology, Cambridge, MA, USA, [3]Now at Department of Liberal Arts, The School of the Art Institute of Chicago, Chicago, IL, USA, [4]Programa de Pós-Graduação em Recursos Naturais da Amazônia, Universidade Federal do Oeste do Pará, Santarém, Brazil, [5]Department of Earth, Ocean & Atmospheric Science, Florida State University, Tallahassee, FL, USA, [6]Department of Marine Geology and Geophysics, Woods Hole Oceanographic Institution, Woods Hole, MA, USA, [7]Departments of Microbiology and Earth and Planetary Sciences, University of Tennessee, Knoxville, TN, USA

Abstract The Amazon River mobilizes organic carbon across one of the world's largest terrestrial carbon reservoirs. Quantifying the sources of particulate organic carbon (POC) to this flux is typically challenging in large systems such as the Amazon River due to hydrodynamic sorting of sediments. Here, we analyze the composition of POC collected from multiple total suspended sediment (TSS) profiles in the mainstem at Óbidos, and surface samples from the Madeira, Solimões and Tapajós Rivers. As hypothesized, TSS and POC concentrations in the mainstem increased with depth and fit well to Rouse models for sediment sorting by grain size. Coupling these profiles with Acoustic Doppler Current Profiler discharge data, we estimate a large decrease in POC flux (from 540 to 370 kg per second) between the rising and falling stages of the Amazon River mainstem. The C/N ratio and stable and radiocarbon signatures of bulk POC are less variable within the cross-section at Óbidos and suggest that riverine POC in the Amazon River is predominantly soil-derived. However, smaller shifts in these compositional metrics with depth, including leaf wax *n*-alkanes and fatty acids, are consistent with the perspective that deeper and larger particles carry fresher, less degraded organic matter sources (i.e., vegetation debris) through the mainstem. Overall, our cross-sectional surveys at Óbidos highlight the importance of depth-specific sampling for estimating riverine export fluxes. At the same time, they imply that this approach to sampling is perhaps less essential with respect to characterizing the composition of POC sources exported by the river.

Plain Language Summary The Amazon River transports one of the largest quantities of freshwater organic carbon into the Atlantic Ocean. In this study, we collected suspended particles at different depths within a cross-section of the Amazon River mainstem during the rising and falling stages of the river's hydrological cycle. We analyzed the organic carbon, nitrogen, grain size, and leaf-derived compounds in these particles, and integrated water velocity measurements to calculate the quantity of carbon in particle form moving through the river at these two stages. The analyses showed that large, dense particles concentrate with depth in the Amazon River mainstem. The composition of these particles is relatively homogenous, but slight variations in metrics like carbon-to-nitrogen ratio, age derived from carbon-dating, and leaf waxes imply that less degraded sources of organic carbon are found in the deeper and coarser grained particles. Overall, the data suggest that the majority of Amazon River particulate organic carbon comes from a mixture of soil organic carbon washing in from different landscapes and soil depth horizons. A globally significant quantity of this carbon will get buried in the Atlantic Ocean, forming a long-term carbon sink.

Key Points:

- Amazon River suspended sediments show little variation in organic carbon composition with depth despite hydrodynamic sorting
- Estimated particulate organic carbon fluxes range from 370 to 540 kg per second during the falling and rising stages, respectively
- The majority of Amazon River particulate organic carbon exported from the mainstem at Óbidos is soil-derived

Supporting Information:

Supporting Information may be found in the online version of this article.

Correspondence to:

S. Z. Rosengard,
srosengard@saic.edu

Citation:

Rosengard, S. Z., Moura, J. M. S., Spencer, R. G. M., Johnson, C., McNichol, A., Steen, A. D., & Galy, V. (2024). Depth-partitioning of particulate organic carbon composition in the rising and falling stages of the Amazon River. *Geochemistry, Geophysics, Geosystems*, *25*, e2023GC011273. https://doi.org/10.1029/2023GC011273

Received 3 OCT 2023
Accepted 28 MAY 2024

Author Contributions:

Conceptualization: Sarah Z. Rosengard, Jose Mauro S. Moura, Robert G. M. Spencer, Valier Galy
Formal analysis: Sarah Z. Rosengard, Carl Johnson, Andrew D. Steen
Funding acquisition: Robert G. M. Spencer, Valier Galy
Investigation: Sarah Z. Rosengard, Robert G. M. Spencer, Valier Galy
Methodology: Sarah Z. Rosengard, Jose Mauro S. Moura, Robert G. M. Spencer, Carl Johnson, Ann McNichol, Andrew D. Steen, Valier Galy

1. Introduction

Of the world's major river networks, the Amazon River Basin, a global biodiversity hotspot, is one of the largest reservoirs of biospheric organic carbon on the planet (Eglinton et al., 2021). The river basin includes eight major tributaries that extend across a 6 million square kilometer drainage basin. Torrential seasonal rains mobilize massive quantities of suspended sediments across flooded and upland rainforests, drier savannahs, high-elevation Andean landscapes, as well as cropland and pasture, into the tributaries and mainstem. As a result, the Amazon

Project administration: Sarah Z. Rosengard, Jose Mauro S. Moura, Robert G. M. Spencer, Valier Galy
Supervision: Robert G. M. Spencer, Ann McNichol, Valier Galy
Visualization: Sarah Z. Rosengard, Valier Galy
Writing – original draft: Sarah Z. Rosengard, Robert G. M. Spencer, Valier Galy
Writing – review & editing: Sarah Z. Rosengard, Jose Mauro S. Moura, Robert G. M. Spencer, Carl Johnson, Ann McNichol, Andrew D. Steen, Valier Galy

River sustains the highest freshwater discharge (Dai & Trenberth, 2002) and one of the largest export fluxes of suspended sediments and particulate organic carbon (POC) to the ocean globally (see compilation by Galy et al. (2015)). The Amazon River Basin's role as a major conduit for POC transport from land to sea has motivated decades of research into its influence on the global carbon cycle and long-term climate (Bouchez et al., 2010, 2014; Hedges et al., 1986; Mayorga et al., 2005; Richey et al., 1990, 2002; Sun et al., 2017; Ward et al., 2013, 2015).

In large river basins, spatial heterogeneity is a significant challenge in quantifying annual basin-wide POC fluxes (Bouchez, Métivier, et al., 2011; Galy et al., 2008; Lupker et al., 2011). The majority of knowledge on riverine particulate geochemistry and POC transport through the Amazon River mainstem has accrued through years of field measurements collected near the municipality of Óbidos in the State of Pará (Figure 1), the most downstream gauging station unaffected by seawater intrusion from the Atlantic Ocean (Kosuth et al., 2009; Moreira-Turcq et al., 2003; Richey et al., 1986). At this location on the mainstem, the Amazon River's particle composition integrates suspended sediments from most of the major tributaries of the drainage basin, particularly the Solimões and Madeira rivers, which join to form the Amazon upstream. At Óbidos, where the mainstem is about 2 km wide and over 60 m deep during some seasons of the year, hydrodynamic sorting can cause larger grain-size sediments to settle faster and concentrate at deeper depths (Bouchez, Métivier, et al., 2011; Curtis et al., 1979; Rouse, 1950), leading to compositional differences between deeper, coarser sediments and shallower, finer sediments (Bouchez, Gaillardet, et al., 2011; Bouchez et al., 2014). In particular, depth-specific differences in total suspended sediment (TSS) concentrations in the mainstem cross-section can span five-fold (Bouchez, Gaillardet, et al., 2011), implying that measurements traditionally based on surface TSS concentrations alone are susceptible to considerable error. For this reason, more recent Amazon POC export flux measurements have integrated sub-surface measurements across depths (e.g., Bouchez, Métivier, et al., 2011; Bouchez et al., 2014; Ward et al., 2015).

Potential depth-dependent differences in organic matter composition in the Amazon River have been explored less, but have implications for our understanding of the sources of organic carbon that are eventually exported to the Atlantic Ocean. Here, we analyze particulate organic matter (POM) from two cross-sectional surveys at Óbidos during two stages of the river's hydrological cycle (i.e., rising and falling water levels), integrating measurements of the bulk POM pool with compound-specific lipid abundances and carbon stable isotope composition. While bulk metrics shed light on the predominant origins of organic matter in the river (Kim et al., 2012; Martinelli et al., 1994; Powell et al., 2012), lipid-specific measurements provide a nuanced understanding of specific carbon sources in the bulk pool, such as terrestrial vegetation and in situ primary production (e.g., Feakins et al., 2018; Häggi et al., 2016; Saliot et al., 2001). Further, following prior studies that have attempted to sample river suspended sediments along transects to understand the loss and replacement of POC from the floodplain to the mouth (e.g., Guyot et al., 1996; Häggi et al., 2016; Hedges et al., 1986; Kim et al., 2012; Sun et al., 2017; Ward et al., 2015), our study also compiles analyses of surface riverine POC samples collected from tributaries both upstream and downstream of our main study location (Óbidos).

To our knowledge, this new data set represents the highest resolution survey of POC within an Amazon River mainstem cross-section, with compound-specific lipid measurements from the surface to within ~15 m above the river bed. Our results expand our understanding of the variability of POM composition in the narrow and deep mainstem of the Amazon River on a spectrum of particle sizes and as a function of seasonality. In addition to contributing this new data set, our study adds a nuanced perspective on the methodology for sampling large, potentially heterogeneous river systems. Our discussion comments on the utility of depth-specific sampling for developing a process-based understanding of POC composition in the Amazon River mainstem. Finally, considering that the tributaries downstream of Óbidos may change the composition of riverine POC exported to the Atlantic Ocean, we conclude by discussing new radiocarbon measurements in suspended sediments from the relatively understudied Tapajós River.

2. Methods

2.1. Overview of Sampling Expeditions

The suspended sediments we discuss in this study were sampled during three expeditions to the Amazon River Basin in June 2005, April 2014, and July 2014 (Table 1, Figure 1). The 2005 samples were collected from the mainstem at Óbidos and at two upstream locations near the Madeira River mouth to the Amazon River (~Foz Madeira) and near the Solimões River confluence with the mainstem (~Manacapuru). The reader may refer to

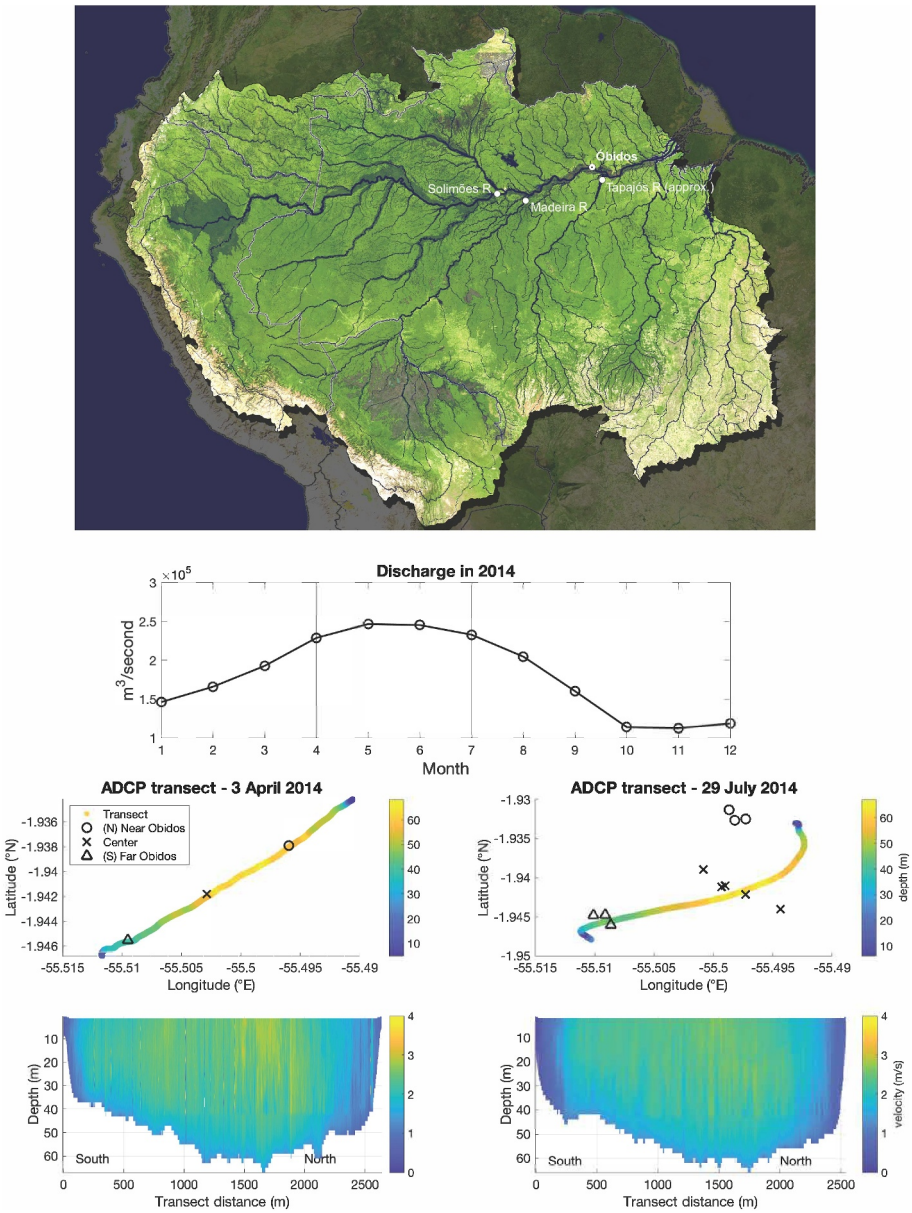

Figure 1. Top row: the Amazon River Basin and all field sites from June 2005, April 2014, and July 2014. Image credit: Paul Lefebvre and Greg Fiske (Woodwell Climate Research Center). Refer to Table 1 for coordinate locations of each sampling site. Second row from top: monthly mainstem discharge time-series in 2014, compiled by the Brazilian Agência Nacional de Águas (https://www.snirh.gov.br/hidroweb/serieshistoricas). Each number represents the average flow measured on the first day of each month of the year (month #1 is January; month #12 is December). The vertical solid lines represent the two sampling months, April and July. Third row from top: Acoustic Doppler Current Profiler (ADCP) transects in latitude/longitude across the Amazon River at Óbidos in April and July 2014, with color indicating river depth. Transects started at the right bank across from Óbidos and ended at the left bank near Óbidos. The markers indicate approximate locations of each TSS sample. Note that exact GPS coordinates of each individual sample were not recorded during the April transect. Bottom row: measured and extrapolated water velocities within the cross-section at Óbidos in April 2014 and July 2014, with the colorbar representing water velocity.

Bouchez, Métivier, et al., 2011 and Supporting Information S1 for more description on the field collection and archival of these 2005 samples. The 2014 samples were collected primarily at Óbidos. Sampling occurred once in the rainy season in March/April, and once in the dry season, July 2014. In July 2014, suspended sediments were also retrieved from the Tapajós River downstream from Óbidos.

Table 1
Sample Locations and Times

River	Location	Latitude (°S)	Longitude (°W)	Date	Channel position (km)	Sample depth (m)	Temperature (°C)	Volume	Discharge (m^3/s)	zR	TSS flux (kg/s)	POC flux (kg/s)
mainstem	Óbidos	1.937[a]	55.503[a]	8 June 2005	–	0	no data	>100 L	128,000	0.39	61,300	604
Madeira	Foz Madeira	3.456[a]	58.808[a]	6 June 2005	–	0	no data	>100 L	21,800	0.10	1,300	14
Solimões	Manacapuru	3.314[a]	60.554[a]	4 June 2005	–	0	no data	>100 L	124,700	0.09	17,400	168
mainstem	Óbidos	1.946	55.510	2 April 2014	0.32	35.49	25.9	~10 L	270,000	0.26	53,000	544
mainstem	Óbidos	1.946	55.510	2 April 2014	0.32	15.3	27.3	~10 L	270,000	0.26	53,000	544
mainstem	Óbidos	1.946	55.510	2 April 2014	0.32	2.1	no data	~10 L	270,000	0.26	53,000	544
mainstem	Óbidos	1.942	55.503	2 April 2014	1.1	49.1	no data	~10 L	270,000	0.26	53,000	544
mainstem	Óbidos	1.942	55.503	2 April 2014	1.1	30.15	27.5	~10 L	270,000	0.26	53,000	544
mainstem	Óbidos	1.942	55.503	2 April 2014	1.1	13.33	26.8	~10 L	270,000	0.26	53,000	544
mainstem	Óbidos	1.942	55.503	2 April 2014	1.1	2.7	26.4	~10 L	270,000	0.26	53,000	544
mainstem	Óbidos	1.938	55.496	2 April 2014	2.00	27.8	27.5	~10 L	270,000	0.26	53,000	544
mainstem	Óbidos	1.938	55.496	2 April 2014	2.00	10.4	26.1	~10 L	270,000	0.26	53,000	544
mainstem	Óbidos	1.938	55.496	2 April 2014	2.00	2.8	26.1	~10 L	270,000	0.26	53,000	544
mainstem	Óbidos	1.940	55.501	1 April 2014	–	0	28.0	>100 L	270,000	N/A	53,000	544
Tapajós	Tapajós	no data	no data	27 July 2014	–	0	no data	>100 L	no data	N/A	no data	no data
Tapajós	Tapajós	no data	no data	27 July 2014	–	bed	no data	N/A	no data	N/A	no data	no data
mainstem	Óbidos	1.946	55.509	28 July 2014	0.34	42.8	28.9	~10 L	249,000	0.34	48,000	369
mainstem	Óbidos	1.945	55.510	28 July 2014	0.34	20.6	no data	~10 L	249,000	0.34	48,000	369
mainstem	Óbidos	1.945	55.509	28 July 2014	0.34	3.5	no data	~10 L	249,000	0.34	48,000	369
mainstem	Óbidos	1.944	55.494	28 July 2014	1.6	54	28.9	~10 L	249,000	0.34	48,000	369
mainstem	Óbidos	1.942	55.497	28 July 2014	1.6	39.83	29	~10 L	249,000	0.34	48,000	369
mainstem	Óbidos	1.941	55.499	28 July 2014	1.6	30.4	28.9	~10 L	249,000	0.34	48,000	369
mainstem	Óbidos	1.941	55.499	28 July 2014	1.6	14.95	no data	~10 L	249,000	0.34	48,000	369
mainstem	Óbidos	1.939	55.501	28 July 2014	1.6	3.14	no data	~10 L	249,000	0.34	48,000	369
mainstem	Óbidos	1.933	55.497	28 July 2014	2.2	53.06	29	~10 L	249,000	0.34	48,000	369
mainstem	Óbidos	1.931	55.499	28 July 2014	2.2	29.83	no data	~10 L	249,000	0.34	48,000	369
mainstem	Óbidos	1.933	55.498	28 July 2014	2.2	3.33	no data	~10 L	249,000	0.34	48,000	369
mainstem	Óbidos	1.942	55.496	28 July 2014	–	0	29.2	>100 L	249,000	0.34	48,000	369
mainstem	Óbidos	no data	no data	28 July 2014	–	bed	no data	N/A	249,000	N/A	48,000	369
mainstem	Óbidos	no data	no data	28 July 2014	–	bed	no data	N/A	249,000	N/A	48,000	369
mainstem	Óbidos	no data	no data	28 July 2014	1	flood	no data	N/A	249,000	N/A	48,000	369

Note. Depth-specific samples at Óbidos were collected in three positions across the mainstem channel, referenced to the right bank across from Óbidos (Figure 1). The 2005 data are taken from Bouchez, Métivier, et al. (2011) and Bouchez et al. (2014). Discharge, total suspended solid (TSS) and particulate organic carbon (POC) fluxes, and water temperatures are provided when available. In the sample depth column, "bed" = bedload and "flood" = floodplain deposit. [a]Latitude & longitude reflect one GPS coordinate for this sampling station and date.

In 2014, mainstem discharge at Óbidos varied by a factor of two between a minimum during the dry season and a maximum during the rainy season (Figure 1b). Continuous gauge measurements near Óbidos (https://www.snirh.gov.br/hidroweb/serieshistoricas), conducted by the Brazilian Agência Nacional de Águas, showed that in 2014, discharge peaked in May and June at ~250,000 m^3/s (Figure 1b). Thus, the two sampling months in 2014 reflect different river stages, rising in April and falling in July, prior to and after peak discharge, respectively.

Each expedition served a unique purpose in this study. The two 2014 expeditions to Óbidos provided the majority of samples we analyze in this study, as well as an opportunity to quantify TSS and POC fluxes during two hydrological stages of the river, using a depth-integrated method complementary to the prior expeditions (Bouchez,

Métivier, et al., 2011). The other samples collected in 2005 and the one Tapajós River sample collected in 2014 allowed for an extended comparison between Amazon River POC at Óbidos and POC from its most immediate upstream and downstream tributaries.

2.2. Particle Collection

All suspended sediments were collected by filtering several large-volume (100–200 L) samples of surface river water and a number of small-volume (∼10 L) samples at specified depths below the surface. The exact volumes were calculated by weighing the water samples after collection and converting mass to volume using the density of fresh water, ∼1 kg/L. With the exception of the 2005 samples, all water samples were filtered in pressurized Teflon-coated units through 0.22 μm diameter pore size Millipore PES membrane filters within 2 days after collection. Between collection and filtration, samples were either covered in a dark tarp or stored in the shade to minimize exposure to sunlight. After filtration, the particles on the filters were immediately frozen on board the ship. Although previous studies have highlighted the compositional differences across particle size fractions in the Amazon River (Aufdenkampe et al., 2007; Hedges et al., 1986, 1994), we have chosen to pool all particles above 0.22 μm in diameter for analysis of the total riverine particle pool, which is just above the 0.1 μm upper limit for sampling dissolved organic matter (Amon & Benner, 1996). Assuming that riverine particles span a spectrum of sizes above 0.1 μm, this choice captures the majority of particulate matter while remaining consistent with particle size ranges in other studies (e.g., Bouchez, Métivier, et al., 2011).

The large-volume samples were acquired at Óbidos (April 2014, July 2014, and June 2005), and each upstream/downstream tributary site using a bucket submerged a few tens of centimeters below the surface. Each sampling location was roughly in the center of each river channel. The 10 L samples were collected within three depth profiles at Óbidos in April and July 2014 using a depth-specific horizontal isokinetic sampler. Each profile, consisting of three to five depths from 2–3 to ∼50 m, was located at a different position in the channel of the mainstem between the right bank and the left bank closer to Óbidos (Figure 1, Table 1). The depth-specific water sampler was equipped with a depth sensor to accurately record the collection depths.

In July 2014, additional bedload samples from the Tapajós River and mainstem at Óbidos were taken using a dredge sampler. One flood deposit sample from the right bank of the mainstem, across from Óbidos, was also collected during this same expedition. Similar to the water-column particle samples, these bedload and flood deposit samples were immediately frozen following collection until analysis.

In the laboratory, each suspended sediment sample was resuspended from the filters in milli-Q water and freeze-dried, while bed samples and the floodplain deposit were directly freeze-dried. All dried samples were sieved through a 2 mm mesh to remove any coarse impurities such as rock fragments and leaf debris, and homogenized before subsequent analyses. The homogenized quantities of suspended sediments were weighed to calculate suspended sediment concentrations (mg/L).

2.3. Flux Calculations

During both sampling trips, on 3 April and 29 July 2014, water velocity profiles were measured across the mainstem channel using a *Sontek RiverSurveyor® M9* Acoustic Doppler Current Profiler (ADCP). The ADCP operated on a 1 MHz frequency, and was equipped with a 0.5 MHz vertical beam sensor for river depth measurements and an external GPS for compass heading, latitude and longitude tracking. The external GPS did not function over most of the transect in April, so an average offset from the external GPS was applied to correct the internal *Sontek* compass, which provided continuous heading measurements. The *RiverSurveyor®* software integrated velocities measured through the instrument's transect and modeled velocities within the "edge" regions between each end of the instrument transect and the nearest river bank to calculate a water discharge value through the river's cross-section.

The velocity cross-sections guided our choice of sample depths and locations for each depth profile (Figure 1, Table 1, Section 2.2) and enabled us to calculate suspended sediment fluxes across the mainstem. The ADCP measured three velocity components (E, N, U) down to 40 m depth. Horizontal velocities, V_{mag}, were calculated as the vector combination of the E (east) and N (north) components. Because 40 m was often shallower than the river bed and a further 10% of each velocity profile data was discarded prior to data export, the deepest measured

Table 2
Substrates for Measuring Enzyme Activities in the Amazon River Mainstem, July 2014

Substrate	Abbreviation	Enzyme	Element
leucine-AMC	Leu-AMC	leucyl aminopeptidase	N
Phenylalanine-AMC	Phe-AMC	phenyalanyl aminopeptidase	N
Ala-Ala-Phe-AMC	AAF-AMC	chymotrypsin	N
MUB-beta-N-acetyl glucosamine	MUB-NAG	N-acetylglucosaminidase	N
MUB-cellobiose	MUB-cello	cellulase	C
MUB-beta glucose	MUB-beta-glu	beta-glucosidase	C
MUB-beta xylose	MUB-xyl	xylanase	C
MUB-PO4	MUB-PO4	phosphomonoesterase	P

Note. AMC is -amino-4-methylcoumarin and MUB is 4-methylumbelliferone.

velocities had to be extrapolated to the river bed using the following relationship between horizontal velocity, V_{mag}, and vertical distance above the river bed z (Chen, 1989; Mueller et al., 2009):

$$V_{mag} = a_v z^{1/6} \quad (1)$$

The a_v values for each ADCP transect position were first extracted by fitting the measured V_{mag} profiles to Equation 1. Then, the extrapolated V_{mag} values for all depths between the deepest measured V_{mag} and the river bed were calculated using the fitted a_v values.

Suspended sediment concentration profiles (C_z) were modeled based on the assumption that the Amazon River mainstem was deep enough in April and July 2014 to allow separation of sediment grain size and density by depth. Following Bouchez, Métivier, et al. (2011), who also reported hydrodynamic sorting in the Amazon mainstem, all depth-specific suspended sediment concentrations from each sampling month were fitted to a Rouse equation, which relates sediment concentration to river depth (Rouse, 1950):

$$\frac{C_z}{C_a} = \left(\frac{H - z}{z}\frac{a}{H - a}\right)^{z_R} \quad (2)$$

In this relationship, C_z is the suspended sediment concentration at z, the vertical distance above the river bed, which has a depth of H. The constant a is the depth of the shallowest point measurement in the depth profile, C_a is the suspended sediment concentration at a, and z_R is the Rouse number. We used a nonlinear least-squares fit to calculate the Rouse number for April and July. The Rouse fits allowed us to model C_z across the entire mainstem cross-section by varying H from the ADCP data, but using constant C_a values, averaged across the surface-most measurement of the three channel positions in each sampling month.

We calculated suspended sediment fluxes at Óbidos during each sampling month by integrating the product of suspended sediment concentration (C_z, modeled by Equation 2) and water velocity (both measured and extrapolated V_{mag} values, according to Equation 1) across channel position and over river depth (Bouchez, Métivier, et al., 2011):

$$\text{TSS flux} = \iint V_{mag} C_z \, dx \, dz \quad (3)$$

In Equation 3, dx values were calculated by projecting the distance of the boat track using ADCP transect coordinates (Figure 1) against the azimuth of the mainstem at Óbidos.

2.4. Enzyme Activity Assays

Enzyme assays were conducted on suspended particles from the July 2014 Óbidos depth profiles to probe variations in heterotrophic activity in the Óbidos cross-section. Samples were analyzed using –AMC (7-amino-4-methylcoumarin) and –MUB (4-methylumbelliferone)-based fluorogenic substrate proxies (Mullen et al., 2018) (Table 2) and buffered with 100 mM carbonate buffer (pH = 6.85). Assays were performed in triplicate for all

samples and for one control, boiled to denature all enzymes, which served as a blank correction. Fluorescence was measured three to four times during 4-hr sample and control incubations in 1 mL cuvettes at ambient temperature. Enzyme activities in each sample were inferred from the blank-subtracted substrate hydrolysis rates calculated from these four time points.

2.5. Bulk Particle Composition

The distribution of grain sizes in the homogenized particle samples (Section 2.2) was analyzed using a Beckman Coulter Laser Diffraction Particle Size Analyzer (LS 13 320). Samples were sonicated for 10 s in tap water before loading into the detector. The LS 13 320 detects particles in the 0.4 μm to 2 mm size range and reports the mean and median grain size for each sample. The software additionally calculates the volumetric contribution of particle sizes throughout the distribution as well as the d10, d50, and d90 diameters, which delineate the 10th, 50th, and 90th percentiles of the size distribution, respectively.

Bulk weight % organic carbon (%OC), weight % total nitrogen (%N), $\delta^{13}C$, and $\delta^{15}N$ in the homogenized suspended and bed sediments were analyzed using a *Fisons Instruments Carlo Erba 1108* elemental analyzer interfaced via a *Finnigan MAT Conflo II* to a *Delta-Plus* Stable Light isotope ratio mass spectrometer (IRMS). Prior to measuring % OC and $\delta^{13}C$, sub-samples were weighed, loaded in silver boats, fumigated in concentrated hydrochloric acid (12 N HCl) vapors for 72 hr at 60°C, and then dried in a desiccator at 60°C for 72 hr to remove the inorganic carbon in the sediment (Whiteside et al., 2011). Due to an error in the methodology, one bedload sediment from Óbidos was analyzed after just 12–16 hr of acid fumigation. Weighed sub-samples were not fumigated prior to measuring %N and $\delta^{15}N$. All analyses were conducted in triplicate. The results only report the average and standard deviation of the triplicate measurements. We equate the error of the average %OC, %N, bulk $\delta^{13}C$ and $\delta^{15}N$ values to the standard deviation of triplicate analyses for each sample.

For bulk radiocarbon composition, sub-fractions of selected sediment samples were similarly decarbonated via acid fumigation for 72 hr. After drying, the fumigated sample was sealed in an evacuated quartz tube with 2 g copper oxide, and baked at 850°C for 6 hr, which converted all the sample organic carbon to CO_2 gas (McNichol et al., 1995). The evolved CO_2 was then cryogenically purified under vacuum, graphitized by iron catalysis in pure H_2 gas at 450°C, and analyzed for its radiocarbon composition at the National Ocean Sciences Accelerator Mass Spectrometry (NOSAMS) facility at Woods Hole Oceanographic Institution (McNichol et al., 1992). Because the relative errors in bulk F_m values were small, ranging from ~0.2% to 0.5%, they are not reported in the following sections.

2.6. Compound-Specific Lipid Analysis

Abundances of specific biomolecules provide higher-resolution details of organic matter composition. Straight-chain *n*-alkanes and fatty acids were quantified in each large-volume sample collected in 2005 and 2014, and in four depth-specific samples collected in 2014 (Table 1). Total lipids were extracted from the sediment into 15–20 mL of 9:1 (v/v) dichloromethane (DCM)/methanol at 100°C for 20 min using a Microwave Accelerated Reaction System (MARS, CEMS Corp.). The total lipid extracts were then saponified in 15 mL of 0.5 M potassium hydroxide (KOH) in wet methanol at 70°C for 2 hr. After adding 20 mL milli-Q water and 0.5 g of sodium chloride to the KOH solution, the basic lipids were extracted from the aqueous phase via five hexane rinses. The remaining KOH solution was acidified to pH ~ 2 using 12 N HCl to isolate the acidic lipids in five rinses with 4:1 (v/v) hexane/DCM.

Each basic and acidic lipid fraction was separated into five biomolecular classes on the basis of polarity. The concentrated lipid fractions were loaded onto aminopropyl silica gel columns and sequentially flushed with hexane (for *n*-alkanes), 4:1 (v/v) hexane/DCM (for ketones), 9:1 (v/v) DCM/acetone (for sterols, alcohols and other polar compounds), 2.6% oxalic acid in methanol (for fatty acids), and 1:1 (v/v) DCM/methanol (for residual compounds). Both acidic and basic fraction-derived fatty acids were re-combined and methylated in 95:5 (v/v) methanol/HCl with a known $\delta^{13}C$ value and ^{14}C composition for 12–16 hr at 70°C. The fatty acid methyl esters (FAMEs) were isolated on an additional aminopropyl silica gel column after methylation.

Prior to compound-specific isotope analysis, large-volume FAMEs and *n*-alkanes were urea-adducted as an additional purification step to separate the branched compounds from straight-chain compounds. For urea adduction, these compound fractions were first mobilized in 2:1 (v/v) hexane/DCM and a 40 mg/mL solution of

urea dissolved in methanol. After being blown down to dryness, the residual urea crystals were washed in hexane and redissolved in water. The branched compounds in this aqueous phase were separated from straight-chain compounds through >2 washes of hexane (for *n*-alkanes) or 4:1 (v/v) hexane/DCM. There was no need to further purify the four depth-specific FAMEs and *n*-alkane fractions that were selected for compound-specific isotope analysis.

All compound abundances were measured using a flame ionization detector coupled to a *Hewlett Packard 5890 Series II* Gas Chromatograph (GC-FID). Urea-adducted, combined acid and base fractions of *n*-alkanes and FAMEs were injected in high purity hexane. In addition, the non-adducted fractions of FAMEs and *n*-alkanes as well as the other fractions of the post-methylation FAMEs were analyzed in the GC-FID. Any "residual" FAMEs and *n*-alkane quantities in these other fractions were added to the FAMEs and *n*-alkane quantities from the purified fractions, and are reported as such in Sections 3 and 4, all Tables S1–S3 and Figures 4–6.

All GC-FID analyses were accompanied by a suite of standard *n*-alkanes and FAMEs to cross-reference sample peak retention times and quantify compound abundances by peak areas. Some analyses were accompanied by just one standard injection at one known concentration, while others were accompanied by injection of three different standard concentrations. When three standard concentration chromatograms were available, standard curves were applied to sample peak areas to estimate the analyte mass (in nanograms). When analyses included just one standard concentration, a response factor, equivalent to the average peak area/ng compound across standard compounds, was used to convert sample peak area to mass. A conservative relative error of ±10% was used for lipid masses per extraction based on the relative standard deviation of standard compound peaks across GC-FID analyses.

The $\delta^{13}C$ values of specific FAMEs and *n*-alkanes were measured using a *HP6890* gas chromatograph fitted with a *Gerstel PTV* and interfaced via a *Finnigan MAT Conflo II* to a *Delta-Plus* IRMS. When compound abundances were sufficient, $\delta^{13}C$ values were measured in duplicate or triplicate, with only average and standard deviation values reported, the latter of which serves as a metric for error.

3. Data

3.1. Mainstem Discharge in 2014

Maximum river depth of the Amazon River mainstem at Óbidos was 67–68 m in both April and July 2014, varying more by channel position than by season (Figure 1). The *M9 RiverSurveyor*® ADCP logged >1,400 velocity profiles from the surface to the riverbed in April and >1,300 profiles in July. The average water velocity across the transect was 2.0 ± 0.6 m/s in April and 1.7 ± 0.6 m/s in July. In both seasons, velocities tended to be highest (3–4 m/s) in the middle of the cross-section, where depths exceeded 40 m. Velocities near the river bed were generally slower, less than 1.5 m/s. Total calculated discharge from integrated velocities (Section 2.3) at Óbidos decreased slightly between sampling months ranging from 270,000 m^3/s in April to 249,000 m^3/s in July (Table 1). While our July value was consistent with measurements from the Brazilian Agencia Nacional de Águas (Figure 1b), our instantaneous April value overestimated the logged discharge at Óbidos by ∼18%.

3.2. TSS Concentrations and Fluxes in 2014

Total suspended sediment concentrations ([TSS]) throughout the main-stem cross-section at Óbidos varied from 55.5 to 318.5 mg/L in April 2014 (Figure 2, Table 3), within the range of all suspended sediment concentrations analyzed at Óbidos in 2005 (Bouchez, Gaillardet, et al., 2011). July values were broader, ranging from 16.4 to 741.4 mg/L. Concentrations were highest in the deepest samples near the right bank (i.e., across from the municipality of Óbidos) in both April and July 2014. Positioned inside of a bend in the Amazon mainstem, a greater abundance of particles accumulates in river waters here, leading to significantly higher TSS concentrations (i.e., greater than mean + 1 S.D. of all other depth-specific [TSS] values). In July, this deep sample has the highest C/N value of all depth-specific samples from the same sampling period, potentially bearing the signature of resuspended organic matter deposits from the adjacent river bank, which has a higher C/N value compared to the other April/July suspended sediments.

Total suspended sediment concentrations increased with depth in all profiles at Óbidos (Figure 2, Table 3). Other than in the right bank profiles in April, mean, median/d50, d10, and d90 grain size diameters generally increased

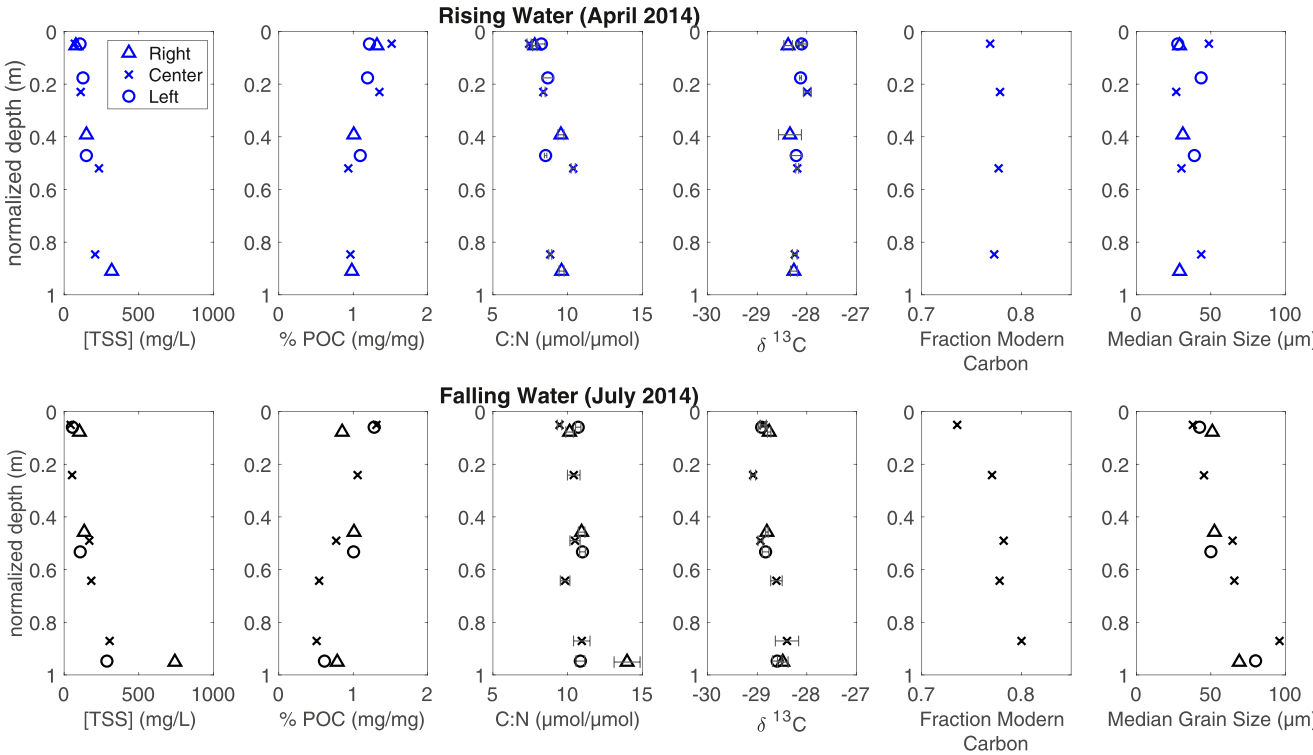

Figure 2. Profiles of TSS concentration, organic matter composition, and median grain size (d50) at Óbidos in April (blue) and July (black) 2014. Data from profiles near the right bank (triangles), left bank (circles) and river center (crosses) are separate. All *y*-axes are normalized to the river depth at the channel position of each profile. The errors in %POC, %PN and fraction modern are relatively small and therefore not plotted. $\delta^{13}C$ values are expressed in units of ‰.

with depth and [TSS], providing clear evidence for hydrodynamic sorting of sediment in the cross-section (Bouchez, Métivier, et al., 2011; Rouse, 1950). All 10 L [TSS] values were fitted to the Rouse equation (C_z in Equation 2). We chose to combine profiles within each sampling month rather than calculate one Rouse number per channel position profile per month, following the reasoning that the errors from fitting individual instantaneous profiles in a given depth profile could be offset by the spatial heterogeneity of three depth profiles spanning the cross-section (Bouchez, Métivier, et al., 2011). The reference height above the river bed, z_a, varied from 36.9 to 56.2 m in April and from 41.5 to 58.9 m in July. The suspended sediment concentration at z_a, C_a, varied from 71.6 to 106.8 mg/L in April and from 43.9 to 102.7 mg/L in July. These TSS concentration fits yielded Rouse numbers of 0.26 and 0.34, respectively, in April and July (Table 1). The modeled concentration profiles fit the data well, suggesting that the Rousean description of hydrodynamic sorting adequately explains our observations (Figure 3).

The integrated product of [TSS] and water velocity within each cross-section yielded instantaneous suspended sediment fluxes of ~53,000 kg/s in April and ~48,000 kg/s in July (Equation 3). We note that while these values do not incorporate water discharge and sediment concentrations within the cross-sectional area between each river bank and the ends of the ADCP transects (i.e., the "edge" discharge values calculated by the RiverSurveyor® software, as described in Section 2.3), discharge in these "edge" sections of the transect represents less than 1% of total discharge at the mainstem.

3.3. Bulk POC Composition

The weight % organic carbon (%OC) within depth-specific sediments at Óbidos ranged from 0.51% to 1.52% and decreased with depth in all profiles across channel positions and seasons (Figure 2, Table 3). Weight % nitrogen (%N) values in suspended sediments ranged from 0.05% to 0.24% and decreased with depth as well. At the same time, particulate organic carbon concentrations ([POC]), which ranged from 0.6 to 5.9 mg/L, increased with depth as TSS concentrations increased. Molar C/N ratios exhibited a large range from 7.4 to 14.0, and tended to increase with depth in all profiles. Even though [TSS], %OC, and [POC] varied within profiles at Óbidos, the isotopic

Table 3
Total Suspended Sediment Concentration, Organic Matter Composition and Grain Size of 2005 and 2014 Samples

Location	Depth (m)	Channel position (km)	[TSS] (mg/L)	%POC (mg/mg)	%PN (%)	C/N (μmol/μmol)	$\delta^{13}C$ (‰)	Fraction modern	Grain-mean (μm)	Grain-d50 (μm)	Grain-d10 (μm)	Grain-d90 (μm)
mainstem[a]	0	–	no data	0.85 ± 0.01	0.14 ± 0.005	7.3 ± 0.5	−28.5 ± 0.05	0.71	no data	no data	no data	no data
Solimões[a]	0	–	no data	1.12 ± 0.06	0.17 ± 0.003	7.9 ± 1.8	−27.0 ± 0.05	0.72	no data	no data	no data	no data
Madeira[a]	0	–	no data	0.49 ± 0.01	0.08 ± 0.0004	7.2 ± 1.9	−27.7 ± 0.3	0.67	no data	no data	no data	no data
mainstem	0	–	55	1.37 ± 0.01	0.19 ± 0.004	8.5 ± 0.2	−28.1 ± 0.06	0.72	no data	no data	no data	no data
mainstem	35.49	0.32	319	0.98 ± 0.02	0.12 ± 0.001	9.6 ± 0.2	−28.3 ± 0.07	no data	44	29	4	109
mainstem	15.3	0.32	150	1.01 ± 0.02	0.12 ± 0.001	9.5 ± 0.2	−28.3 ± 0.2	no data	48	31	5	121
mainstem	2.1	0.32	79	1.32 ± 0.02	0.20 ± 0.001	7.8 ± 0.1	−28.4 ± 0.09	no data	50	29	4	131
mainstem	49.1	1.1	208	0.96 ± 0.01	0.13 ± 0.001	8.8 ± 0.1	−28.2 ± 0.05	0.77	63	44	6	153
mainstem	30.15	1.1	233	0.93 ± 0.01	0.11 ± 0.001	10 ± 0.1	−28.2 ± 0.03	0.78	48	30	5	119
mainstem	13.33	1.1	111	1.35 ± 0.01	0.19 ± 0.002	8.4 ± 0.1	−28.0 ± 0.08	0.78	43	27	4	106
mainstem	2.7	1.1	72	1.52 ± 0.01	0.24 ± 0.004	7.4 ± 0.1	−28.1 ± 0.03	0.77	70	49	4	171
mainstem	27.8	2.00	149	1.09 ± 0.01	0.15 ± 0.001	8.5 ± 0.1	−28.2 ± 0.1	no data	61	39	5	154
mainstem	10.4	2.00	126	1.19 ± 0.05	0.16 ± 0.003	8.7 ± 0.4	−28.1 ± 0.02	no data	60	43	6	142
mainstem	2.8	2.00	107	1.22 ± 0.03	0.17 ± 0.002	8.2 ± 0.3	−28.1 ± 0.1	no data	44	28	4	110
Tapajós	bed	–	N/A	0.14 ± 0.002	0.017 ± 0.0003	10 ± 0.3	−29.4 ± 0.2	1.02	no data	no data	no data	no data
Tapajós	0	–	0.52	15.71 ± 0.13	2.69 ± 0.005	6.8 ± 0.1	−31.0 ± 0.1	0.89	no data	no data	no data	no data
mainstem	0	–	16	1.80 ± 0.02	0.23 ± 0.003	9.0 ± 0.1	−29.1 ± 0.06	0.77	no data	no data	no data	no data
mainstem	42.8	0.34	741	0.79 ± 0.04	0.07 ± 0.002	14 ± 0.9	−28.5 ± 0.1	no data	80	69	11	165
mainstem	20.6	0.34	135	1.01 ± 0.003	0.11 ± 0.002	11 ± 0.2	−28.8 ± 0.03	no data	71	52	9	163
mainstem	3.5	0.34	103	0.85 ± 0.02	0.10 ± 0.001	10 ± 0.3	−28.8 ± 0.03	no data	66	51	8	146
mainstem	54	1.6	305	0.51 ± 0.02	0.054 ± 0.001	11 ± 0.5	−28.4 ± 0.2	0.80	106	96	15	212
mainstem	39.83	1.6	182	0.54 ± 0.01	0.064 ± 0.002	9.8 ± 0.3	−28.6 ± 0.1	0.78	80	66	9	176
mainstem	30.4	1.6	169	0.77 ± 0.02	0.086 ± 0.001	11 ± 0.3	−28.9 ± 0.05	0.78	77	65	9	168
mainstem	14.95	1.6	53	1.06 ± 0.02	0.12 ± 0.004	10 ± 0.4	−29.1 ± 0.05	0.77	60	45	7	139
mainstem	3.14	1.6	44	1.31 ± 0.02	0.16 ± 0.002	9.5 ± 0.2	−28.9 ± 0.06	0.74	55	38	6	133
mainstem	53.06	2.2	286	0.61 ± 0.01	0.066 ± 0.001	11 ± 0.3	−28.6 ± 0.1	no data	93	80	13	194
mainstem	29.83	2.2	108	1.00 ± 0.01	0.11 ± 0.001	11 ± 0.2	−28.8 ± 0.07	no data	71	50	8	171
mainstem	3.33	2.2	56	1.28 ± 0.02	0.14 ± 0.0003	11 ± 0.2	−28.9 ± 0.07	no data	62	42	7	153
mainstem	flood	0	N/A	0.50 ± 0.03	0.048 ± 0.001	12 ± 0.9	−28.1 ± 0.08	no data	no data	no data	no data	no data
mainstem	bed	0	N/A	0.064 ± 0.002	0.0093 ± 0.0004	8.0 ± 0.5	−26.6 ± 0.09	0.60	no data	no data	no data	no data
mainstem	bed	0	N/A	0.022 ± 0.001	BDL	no data	−26.9 ± 0.02	0.87	no data	no data	no data	no data

Note. Channel position for depth-specific samples at Óbidos are referenced to the right bank across from Óbidos (Figure 1). Errors for C/N and $\delta^{13}C$ are reported. Relative errors of depth-specific F_m values are <1% and are not reported. BDL = below detection limit; "bed" = bedload; "flood" = floodplain deposit. [a]2005 samples (refer to Table 1 for specific sampling dates).

composition of organic carbon in the sediments did not vary significantly with depth. $\delta^{13}C$ values ranged from −29.1‰ to −28.0‰ across all profiles and seasons, while $\delta^{15}N$ values ranged from 3.1 to 4.3‰. The range in fraction modern (F_m) values was also relatively small (0.74–0.80), corresponding to a radiocarbon age span of 680 years (1,790–2,470 ^{14}C years).

The composition of POC and particulate nitrogen in all mainstem surface samples collected in 2005 and 2014 was similar to the POC composition of the depth-specific samples from 2014. The only difference was that the POC in these surface samples was consistently older, with F_m values as low as 0.71 (2,760 ^{14}C years), than the POC

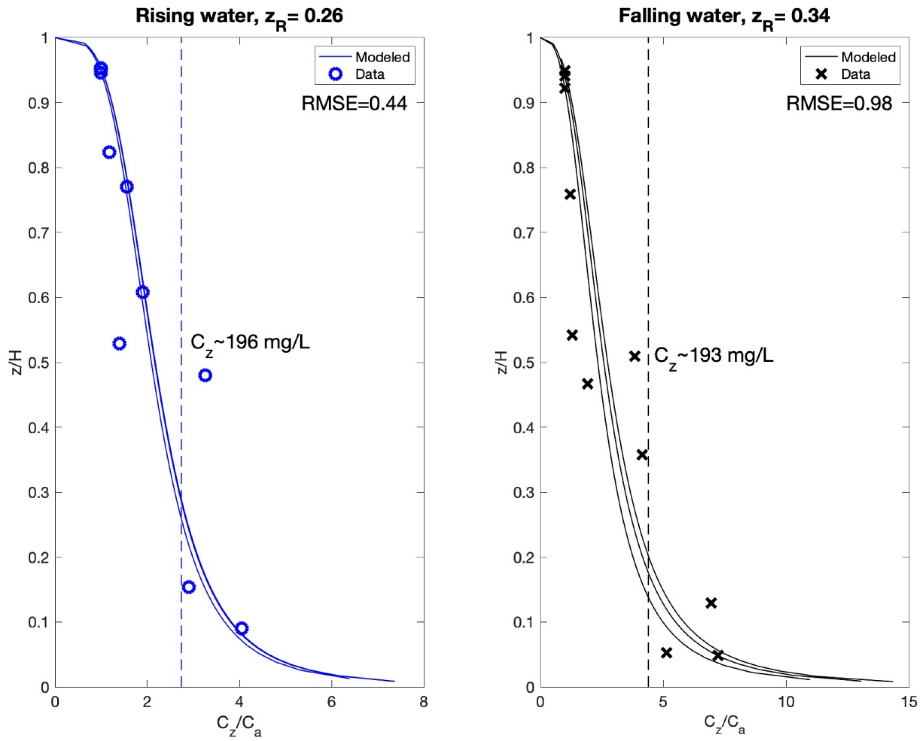

Figure 3. Fits of all depth-specific TSS concentration (C_z) profiles measured at Óbidos in 2014 to the Rouse Equation (Equation 2; Bouchez, Métivier, et al., 2011; Rouse, 1950). Variable z is the height above the river bed H of each profile, and C_a is the surface-most measured C_z value of each profile. The vertical lines corresponding to $C_z \sim 196$ and 193 mg/L are the sediment concentrations needed to compute equivalent sediment fluxes based on sampling at a single (50%) depth.

analyzed at specific depths. Surface suspended sediment concentrations in the Solimões and Madeira rivers, collected in 2005, were also similar to the range observed at Óbidos (Bouchez, Métivier, et al., 2011). The % OC in these sediments ranged from 0.49% in the Madeira River to 1.12% in the Solimões River (Table 3). Weight %N ranged from 0.08% in the Madeira River to 0.17% in the Solimões River. Stable carbon isotope measurements of POC in the Solimões and Madeira River sediments were 0.3–1.1‰ more ^{13}C-enriched than the average δ^{13}C value of depth-specific samples from Óbidos. Fraction modern values in these samples were 0.05–0.11 units lower than the average F_m value of the Óbidos samples. The Tapajós River had the most compositionally distinct suspended sediments of the data set. Surface suspended sediment concentrations in July 2014 were much lower than those observed in any other river, only 0.52 mg/L. Conversely, the %OC in these sediments was the highest measured, 15.7%. Weight %N was also high, 2.69%. The F_m value was 0.89 (955 ^{14}C years), corresponding to a younger ^{14}C age than any of the values measured at Óbidos.

The weight %OC and %N in the three bed sediment samples from near the left bank of Óbidos, the right bank of Óbidos, and the Tapajós River were lower than the corresponding values in all suspended sediment samples, ranging from 0.022% to 0.14% organic carbon and from 0.0027% to 0.017% nitrogen, consistent with other bedload observations in the basin (Bouchez et al., 2014) (Table 3). The δ^{13}C values of bed samples at Óbidos and in the Tapajós River were consistently more ^{13}C-enriched (by ~1–2‰) than POC in suspended sediments in their respective rivers. While radiocarbon ages in the Óbidos bed samples ranged from F_m 0.60 (4,090 ^{14}C years) to 0.87 (1,100 ^{14}C years), we neglect the higher F_m value (0.87) on the basis of specimen contamination (e.g., fresher plant litter debris), as bed samples with such low %OC are typically older across the Amazon River Basin (Bouchez et al., 2010). The Tapajós bed sample was modern ($F_m > 1.0$) and younger than POC in the Tapajós suspended sediment. Values of %OC and %N of the right bank flood deposit near the Óbidos cross-section were more similar to the range in depth-specific sediments, 0.50% and 0.048%, respectively. The stable isotope composition of the flood deposit was closer to the range observed across depth-specific suspended sediment samples, as well.

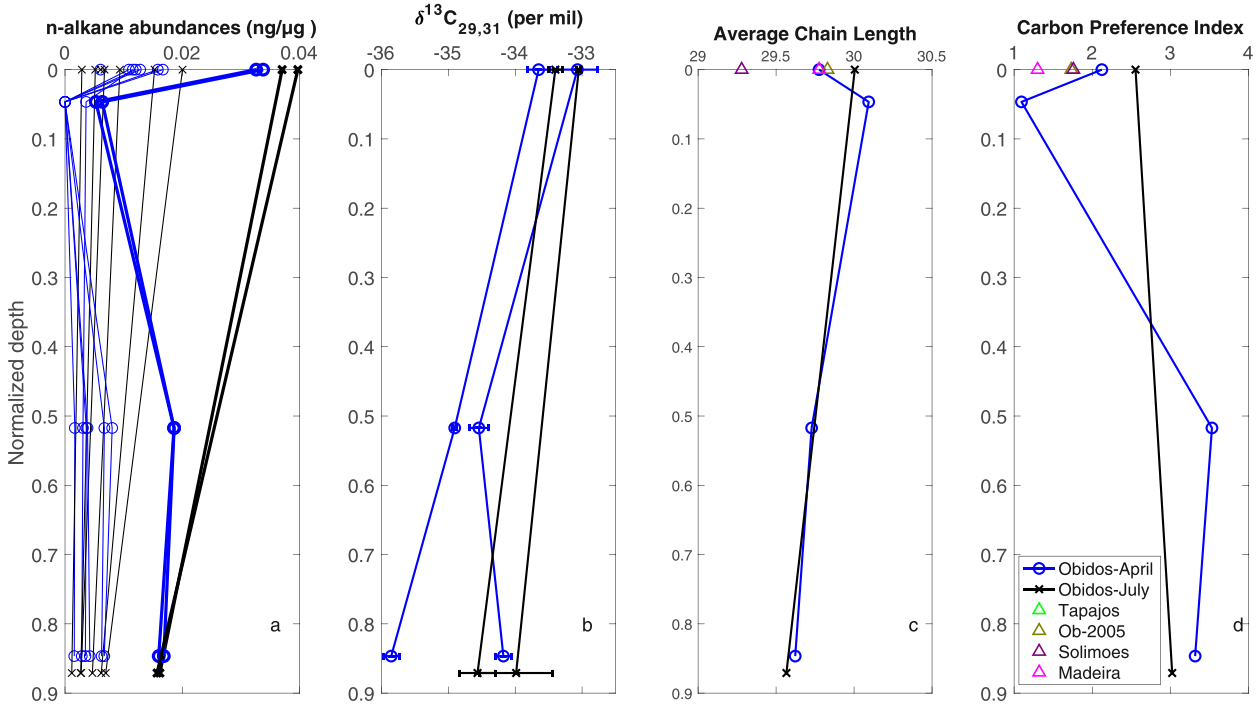

Figure 4. Depth profiles of *n*-alkane (a) abundances (ng/µg total particulate organic carbon), (b) $\delta^{13}C$ values (‰), (c) average chain lengths (ACL), and (d) carbon-preference index (CPI) measured in Óbidos center profiles in April 2014 (blue) and July 2014 (black). Additional ACL and CPI values for surface samples at Óbidos in 2005 and different river tributaries are plotted as well. Different lines in (a) plot values for a different chain length between 19 and 35. The thicker width lines in (a) plot chain lengths 29 and 31 only, highlighting the highest abundance *n*-alkanes.

3.4. Lipid Abundances and Isotope Composition

Measurements of leaf wax compounds provide a useful tool for tracing POC sources in complex mixtures such as riverine sediments. Alongside our other analyses, these lipid abundances and carbon stable isotopes enable a more nuanced understanding of the organic matter pools that contribute to bulk POC among different sampling seasons and tributary locations. Total lipids were extracted from all large-volume suspended sediment samples from the surface of the Amazon River mainstem (June 2005, April 2014, and July 2014), the Tapajós River (July 2014), the Solimões River (June 2005) and the Madeira River (June 2005), as well as from four depth-specific samples from the two 2014 Óbidos center profiles (Table 1). Compound-specific $\delta^{13}C$ values were not resolved for the April 2.7 m sample because the total lipid extract was too small. Compound-specific $\delta^{13}C$ values were also not measured in *n*-alkanes in the tributary samples.

Abundances of straight-chain *n*-alkanes in Óbidos samples were quantified for 16 carbon chain lengths from 19 (C_{19}) to 35 (C_{35}), and ranged from 0.001 to 0.4 ng/µg of total POC (Table S1, Figures 4a, 5c, and 5e). Generally, POC-normalized compound abundances at Óbidos were greater at the surface than abundances measured deeper in the water column. Compared to bulk values, stable isotope values of odd chain-length *n*-alkanes spanned a larger range across months and depths than all $\delta^{13}C$ values measured in bulk POC from the Óbidos depth profiles, ranging from −37.3‰ to −28.3‰ (Figure 4b, Table S1). Generally, lipids at the surface were more ^{13}C-enriched than lipids at deeper depths.

Average chain lengths (ACL) for *n*-alkanes (Equation 4a, Figure 4c) spanned a small range from 29.6 to 30.1, decreasing slightly with depth. The distribution of abundances above chain lengths C_{23} displayed an odd-over-even carbon chain length predominance in all Óbidos samples, characteristic of terrestrial vegetation (Eglinton & Hamilton, 1963) (Figures 5c and 5e). Carbon-preference index (CPI) values (Equation 4b, Figure 4d) ranged from 1.1 to 2.6 at depths of 0–3 m and from 3.0 to 3.5 at depths of 30–54 m across both sampling seasons. In general, lower CPI values, such as those associated with our surface samples, reflect weaker odd-over-even predominance and may be indicative of microbial reworking of *n*-alkanes and petrogenic contributions (Häggi

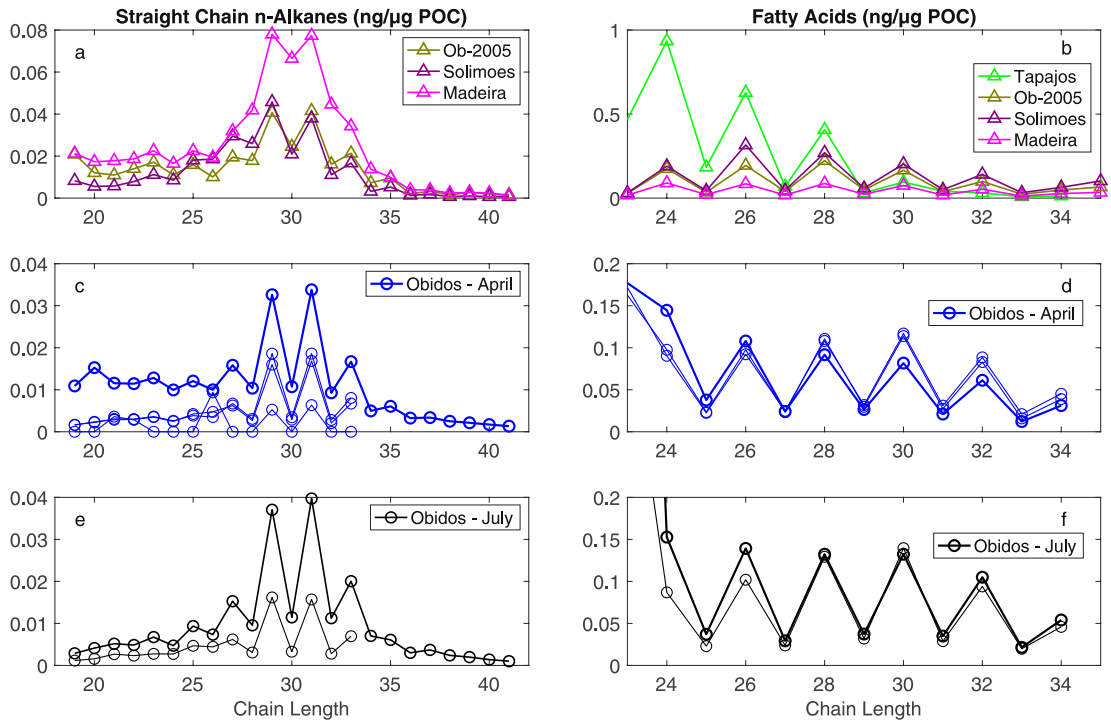

Figure 5. Abundances of (a, c, e) straight chain *n*-alkanes and (b, d, f) fatty acids measured in the Amazon River mainstem and tributaries over a range of longer chain lengths. Each line in the Óbidos April and July panels plots data from a different depth of the center profile, with the boldest line indicating data from the surface large-volume sample.

et al., 2016; Wu et al., 2019). These low CPI values in these samples could also be influenced by petroleum contamination, but there are no other indications in the data set to confirm this, such as petroleum-derived hopane/sterane data (Volkman et al., 1992), anomalously low bulk F_m values, anomalously low compound-specific *n*-alkane F_m values, or significantly different $\delta^{13}C$ values for odd versus even chain-length *n*-alkanes.

$$\mathrm{ACL}_{n-\mathrm{alkane}} = \frac{25[C_{25}] + 27[C_{27}] + 29[C_{29}] + 31[C_{31}] + 33[C_{33}] + 35[C_{35}]}{[C_{25}] + [C_{27}] + [C_{29}] + [C_{31}] + [C_{33}] + [C_{35}]} \tag{4a}$$

$$\mathrm{CPI}_{n-\mathrm{alkane}} = 0.5 \times \left[\frac{[C_{23}] + \ldots [C_{33}]}{[C_{22}] + \ldots [C_{32}]} + \frac{[C_{23}] + \ldots [C_{33}]}{[C_{24}] + \ldots [C_{34}]}\right] \tag{4b}$$

$$\mathrm{ACL}_{\mathrm{fattyacid}} = \frac{24[C_{24}] + 26[C_{26}] + 28[C_{28}] + 30[C_{30}] + 32[C_{32}] + 34[C_{34}]}{[C_{24}] + [C_{26}] + [C_{28}] + [C_{30}] + [C_{32}] + [C_{34}]} \tag{4c}$$

Relative abundances of straight chain *n*-alkanes in surface suspended sediments of the Solimões River were similar to relative abundances observed in the Óbidos samples (Figure 5a), while Madeira River *n*-alkane abundances were higher than both Óbidos and Solimões River samples, particularly for chain lengths 28 to 33. While *n*-alkanes from the Solimões River exhibited odd-over-even predominance, as observed in the mainstem, the odd-over-even predominance in the *n*-alkanes from the Madeira River was weaker (CPI = 1.3). Average chain lengths in all Óbidos and Madeira River samples were similar, while ACL values for the Solimões River sample were lower 29.3 (Figure 4c).

Abundances of saturated straight-chain fatty acids (C_{14}–C_{34}) measured at Óbidos ranged from 0.008 to 4.0 ng/µg POC (Figures 5d and 5f, Table S2). In most samples, the most abundant compounds were C_{16} and C_{18} (0.18–4.0 ng/µg POC). At chain lengths above 22, the abundances exhibited strong even-over-odd predominance in all samples. Differences in relative fatty acid abundances at different sampling months and across depths were negligible, though notable spillage of the large-volume surface sample collected in July could have depressed

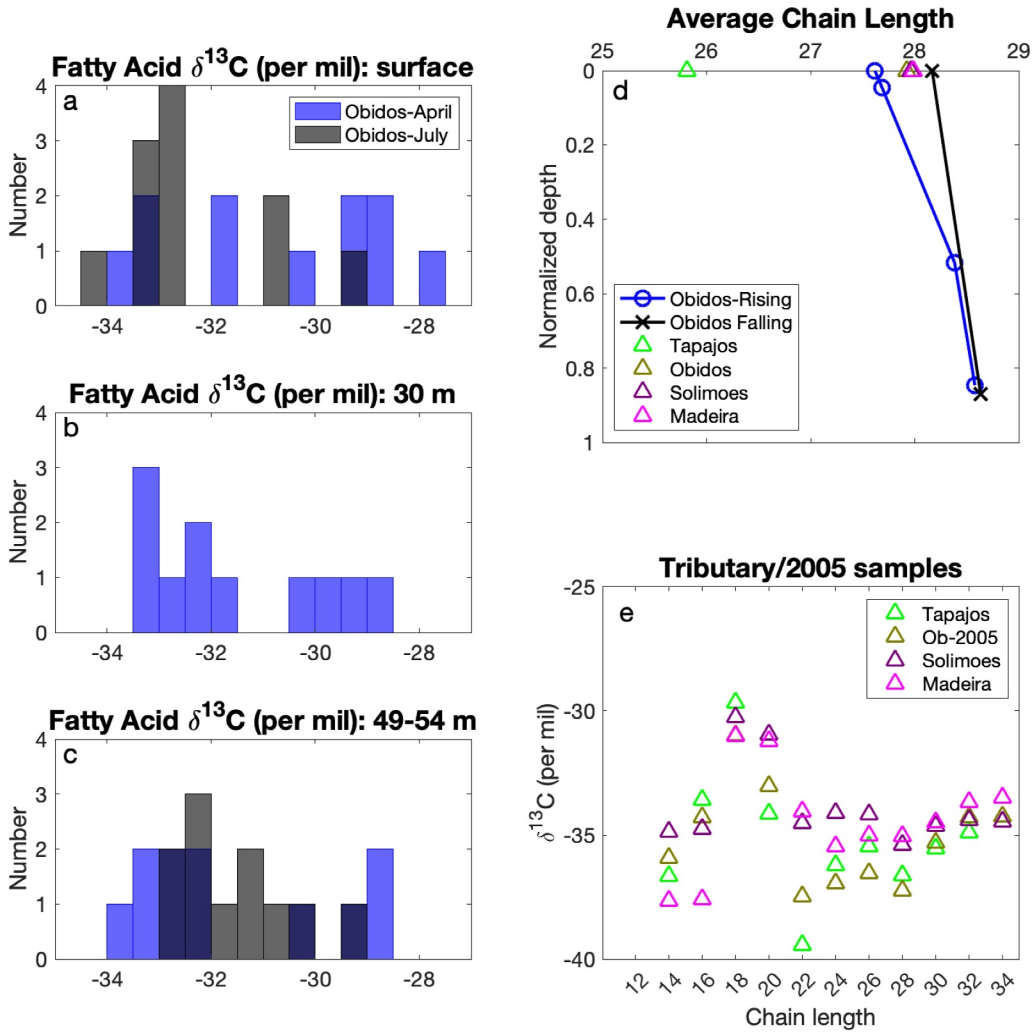

Figure 6. (a–c) Histogram distributions of $\delta^{13}C$ values (‰) and (d) profiles of average chain lengths (ACL) in fatty acids from mainstem samples collected in April (blue) and July (black) 2014. The histograms (a–c) plot values for chain lengths 14–34 at three different depths, showing minor trends in distribution with depth. In (d), additional ACL values are plotted for the surface samples taken from the Tapajós, Solimões, and Madeira Rivers, and from the mainstem in 2005. Panel (e) plots fatty acid $\delta^{13}C$ values in these tributary and mainstem samples over chain lengths 14–34.

abundances quantified by the FID. Average chain lengths of fatty acids (Equation 4c, Figure 6d) did increase with depth from 27.6 near the surface to 28.6 at 49 m in April 2014, and to a lesser extent from 28.2 near the surface to 28.6 at 54 m in July 2014. The stable carbon isotope composition of even chain-length fatty acids across the depth-specific samples spanned a greater range than bulk $\delta^{13}C$ values in the same samples, from −37.5‰ to −27.7‰ (Figures 6a–6c). The $\delta^{13}C$ values were more ^{13}C-enriched with depth for some chain lengths in July samples (i.e., 22, 26, and 28), and more ^{13}C-depleted with depth for other chain lengths in April samples (i.e., 24 and 26).

Straight-chain fatty acids were also quantified in surface suspended sediment samples from the Tapajós, Solimões and Madeira rivers. The upstream tributary samples displayed strong even-over-odd predominance among the higher chain-length fatty acids (Figure 5b). Fatty acid abundances and ACL values generally exhibited a range similar to the Óbidos samples (Table S2, Figures 5 and 6d). Only the Tapajós River sample showed very elevated concentrations of C_{14}, C_{16}, and C_{18} that were up to ∼100 times higher than the abundances of these fatty acids across all other 2014 and 2005 samples, yielding the lowest ACL calculated in the data set (25.8). Compound abundances from chain lengths 24 to 28 in the Tapajós River were also significantly elevated relative to Óbidos, and Solimões and Madeira River samples. By contrast, differences in $\delta^{13}C$ values among Tapajós and other river samples were smaller. Even though the bulk POC from the Tapajós River is relatively ^{13}C-depleted, only $\delta^{13}C$

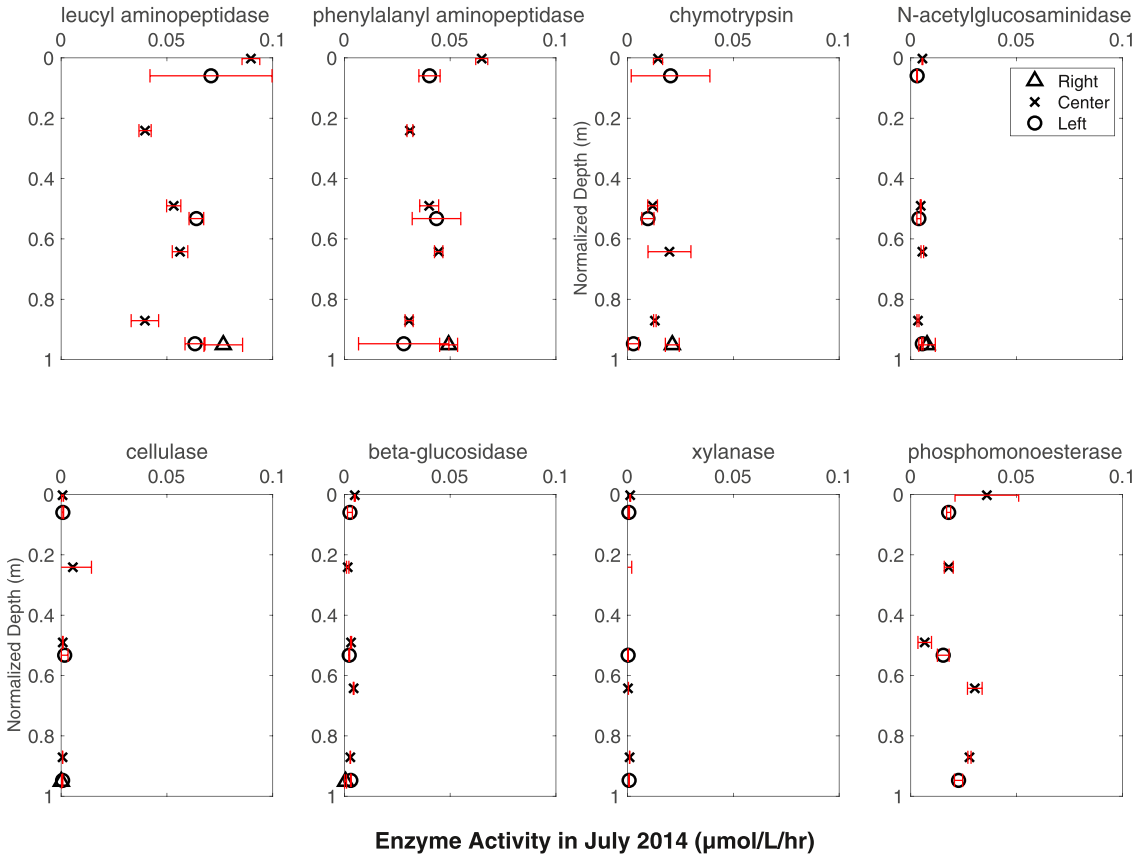

Figure 7. Activities of eight enzymes measured within the Óbidos cross-section in July 2014.

values of C_{20} and C_{22} fatty acids were more than 1‰ ^{13}C-depleted than respective values in Óbidos and other tributaries samples (Figure 6e).

3.5. Enzyme Activities

Activities of eight extracellular enzymes measured at various depths within the Óbidos cross-section in July 2014 ranged from 0 to 0.09 µmol/L-hr (Table S3, Figure 7). Values generally did not vary with depth or channel position. Activities of the N- and P-yielding enzymes (i.e., leucyl aminopeptidase, phenylalanyl aminopeptidase, and phosphomonoesterase) (Table 2) exceeded activities of the C-yielding enzymes (i.e., cellulase, beta-glucosidase and xylanase) throughout profiles.

4. Discussion

The current study offers a cross-sectional survey of suspended particulate organic matter (POM) composition from the mainstem of the Amazon River during two stages of the river's annual hydrological cycle, 1–2 months before and after peak discharge. It is important to note that in the following analyses of the total organic carbon pool and compound-specific biomarkers in particulate organic carbon (POC), measurements represent a mixture of numerous carbon sources with diverse origins and degradation histories. The purpose of the current study is to interpret the predominant sources of organic matter that drive the composition of POC exported through the river cross-section, the processes that may cause them to shift within the parameters of this study (i.e., river depth and season), and the implications such data have on the utility of depth-specific sampling in the Amazon River mainstem.

4.1. Export Flux Comparisons

Increasing TSS concentrations with depth in all profiles compiled at Óbidos in April and July 2014 are indicative of hydrodynamic sorting (Rouse, 1950), and consistent with prior depth profiles of the same size-fraction of sediments compiled by Bouchez, Métivier, et al. (2011) across the central Amazon River Basin (Figures 2 and 3). This sorting effect is supported by even lower TSS concentrations in the surface large-volume samples (<1 m depth) (Table 3). Despite the lack of change in river discharge between April and July 2014, z_R values increased by 0.08 units from 0.26 to 0.34. The Rouse numbers that we report are similar in magnitude and temporal variation to the numbers estimated from profiles at Óbidos in March 2006 ($z_R = 0.24$) and June 2005 ($z_R = 0.39$) (Bouchez, Métivier, et al., 2011).

Increases in grain sizes with depth in July 2014 sediment profiles relative to April 2014 profiles (Student's *t*-test, $p < 0.05$) could have enhanced the depth gradient in July sediment concentrations, leading to higher z_R values. This is consistent with a Ganga River study (Lupker et al., 2011), which partitioned and modeled Rouse profiles of suspended sediment concentrations by grain size, reporting higher z_R values for profiles plotting concentrations of larger grain sizes. Several factors could have increased the grain size of Amazon River suspended sediments between April and July. Of the three major tributaries upstream of Óbidos, variations in the sediment-rich Solimões and Madeira Rivers contribute disproportionately to seasonal variations in sediment grain size in the mainstem, relative to the sediment-poor Negro River (Kim et al., 2012). Although we do not have 2014 grain size data from these upstream tributaries, Bouchez, Métivier, et al. (2011) reported higher median grain diameters in the Solimões River relative to the Madeira River. Therefore, a higher relative discharge from the sediment-rich Solimões River in July, as recorded by the Agência Nacional de Águas, would result in a larger gradient in [TSS] between the river surface and river bed in July. In addition, as will be discussed in Sections 4.2 and 4.3, variations in the POC source could further add to these differences in particle size from April to July, particularly the contribution of larger organic debris from the floodplain.

Overall, our TSS flux estimates (53,000 kg/s in April and 48,000 kg/s in July) are similar in magnitude, though less variable, to fluxes estimated by Bouchez, Métivier, et al. (2011) in June 2005 and March 2006 (61,300 and 39,700 kg/s, respectively) (Table 1). They generally diverge from studies that estimate flux by multiplying discharge by TSS concentration at a single depth. For example, our fluxes are more than five times greater than high water fluxes calculated by Kim et al. (2012) during two expeditions to Óbidos in 2005 and 2009 (~8 tons/s or 7,300 kg/s). Computing sediment fluxes equivalent to ours as the product of discharge and [TSS] from a single depth requires TSS concentrations of 196 mg/L in April and 193 mg/L in July, much greater than surface values reported in Kim et al. (2012). Interestingly, other studies at Óbidos have focused on sampling TSS at the midpoint depth rather than at the river surface (Ward et al., 2015). As Figure 3 illustrates, these target concentrations are greater than our modeled Rousean TSS values at their midpoint depths, though some of our discrete midpoint samples are close to 196 and 193 mg/L. Importantly, these juxtapositions are incomplete in that both Kim et al. and Ward et al. sampled particles in different years and within different pore size intervals, >0.7 μm and 0.45–63 μm, respectively, compared to >0.2 μm in this study.

Particulate organic carbon concentrations increased with depth alongside TSS. We calculated POC fluxes during each sampling month by linearly regressing [POC] against [TSS] (Equation 5) using a Type II regression function in Matlab. This yielded a slope (mg [TSS]/mg [POC]) and intercept (mg/L [POC]) which can then be substituted into the Rouse-modeled C_z in Equation 2:

$$[\mathrm{POC}] = m[\mathrm{TSS}] + b \tag{5}$$

In this equation, m is the slope of the linear relationship (0.0079 mg POC/mg TSS in April and 0.0072 mg POC/mg TSS in July) and b is the intercept (0.46 mg POC in April and 0.075 mg POC in July). The integrated POC flux in April 2014 was 544 kg/s, while the integrated POC flux in July 2014 was 369 kg/s (Table 1). This difference is larger than the difference between TSS fluxes during both months, and can be explained by a significant decrease in the average %OC in depth-specific suspended sediments from 1.16 ± 0.2% (mean ± 1 S.D.) in April to 0.88 ± 0.27% in July (Student's *t*-test, $p < 0.05$). Scaling 544 or 369 kg/s to 1 year results in a flux of ~12–17 Tg/year, though these values are likely overestimates because fluxes could be much lower during lower discharge periods (Moreira-Turcq et al., 2003). Compared to the TSS flux comparisons, these POC fluxes diverge less from previous studies. Again, our instantaneous fluxes are similar to those reported in Bouchez et al. (2014) but ~3–4

times higher than those reported by Kim et al. (2012) during high water. Interestingly, they are close in value to instantaneous POC fluxes reported by Moreira-Turcq et al. (2003), who used a single mean POC concentration to calculate flux. Furthermore, our annual fluxes are similar to earlier flux estimates of 14 Tg/year by Richey et al. (1990), who deployed a depth-integrated sampler to measure POC concentrations (Richey et al., 1986).

Overall, these flux comparisons highlight the importance of accounting for cross-sectional variation and hydrodynamic sorting when estimating TSS and POC exports in the Amazon River main stem. The impact of this methodology on TSS flux calculations is particularly high when considering and comparing numbers across studies. But, cross-sectional sampling is potentially less impactful for calculating POC fluxes; our calculated fluxes were not consistently different from past studies that estimated POC concentration from other depth integration methods. One possible reason is that POC concentrations are affected not only by the total suspended sediment load but also by the %OC values in these particles, which tend to decrease with depth (Figure 2) alongside increases in particle size and decreases in mineral surface area (Bouchez et al., 2014).

4.2. Vertical Distributions in POM Composition

Despite the clear hydrodynamic sorting of sediment and POC concentrations in the mainstem, POC composition is less variable throughout both cross-sectional surveys in April and July 2014, as changes in C/N and carbon isotope composition ($\delta^{13}C$ and F_m) are smaller than changes in [TSS] (Table 3, Figure 2). In their 2005 expeditions to Óbidos, Kim et al. (2012) noted a similar homogeneity in C/N and carbon isotope composition with depth. The lack of large depth-specific variations in bulk POC composition is one likely reason that enzyme activities were homogenous throughout the cross-section at Óbidos as well (Figure 7), supporting an argument that the homogenous organic matter composition throughout the mainstem controls enzyme activities to a greater extent than changes in particle surface area/grain size and TSS concentrations. Importantly, the invariable enzyme activities do not negate the influence of particle-microbe interactions on the metabolism of organic matter in mainstem waters (Satinsky et al., 2014). Indeed, incubation studies have reported a relationship between microbial respiration rates and water velocity in Amazon River water samples (Ward et al., 2018, 2019), the latter of which does span a large range with depth (Figure 1). Furthermore, if these enzyme activities are free-living, detached from bacterial cells in the aquatic environment, or associated with DOC respiration, they are not likely to correlate with or serve as a proxy for changes in microbial respiration in the water column (Baltar, 2018). Given that our results comprise the first measurement of enzyme activities in the Amazon River mainstem, we suggest further exploration of enzyme activities to understand in situ microbial dynamics in relation to sediment sorting and POC composition in the mainstem and tributaries.

There are, however, a few notable differences in POC composition across sample depths and a variety of measurements suggest that such differences reflect a decrease in the degradation state of organic carbon from surface to deep. This is particularly notable in July 2014, when fraction modern values were lowest in surface POC samples and highest in deeper samples (Figure 2). Although the bed load sample at Óbidos still exhibits the oldest bulk carbon signature (lowest F_m) value, consistent with F_m profiles in Bouchez et al. (2010), these data point to an accumulation of fresher (i.e., less degraded) organic matter just above the river bed. Both bulk C/N ratios and *n*-alkane measurements (abundances, stable carbon isotope composition and CPI values) further corroborate this argument. The small increase (~16%) in center profile C/N ratios with depth, and an even larger increase (~40%) within profiles near the right bank in July, implies a shift toward fresher degradation states and greater input of vegetation debris with depth (Hedges et al., 1986; Ometto et al., 2006). Decreases in $\delta^{13}C$ values of C_{29} and C_{31} *n*-alkanes from surface to deep and increases in CPI values with depth (Figure 4) fit the perspective that this deeper POC comes from fresher C3 vegetation, while a pool of more degraded, microbially reworked leaf wax compounds concentrates at the surface (Feakins et al., 2018; Häggi et al., 2016; Wu et al., 2019). A concurrent decrease in POC-normalized C_{29} and C_{31} abundances with depth additionally suggests that the *n*-alkanes near the surface may represent a greater range of degraded source material from across the catchment area, as opposed to a more localized fresh source observed at depth (Hemingway et al., 2016).

Coupled with grain size profiles (Figure 2), these depth-specific differences in POC composition suggest that fresher organic matter pools are exported in coarser particles, and are associated with higher z_R values, as observed in our July 2014 Rouse fits (Section 4.1) (Feakins et al., 2018). By contrast, finer particle size fractions carry old and/or more degraded organic matter, remaining homogenous throughout the water column and lowering z_R values in TSS profiles (Bouchez et al., 2010; Lupker et al., 2011), which is especially apparent in the

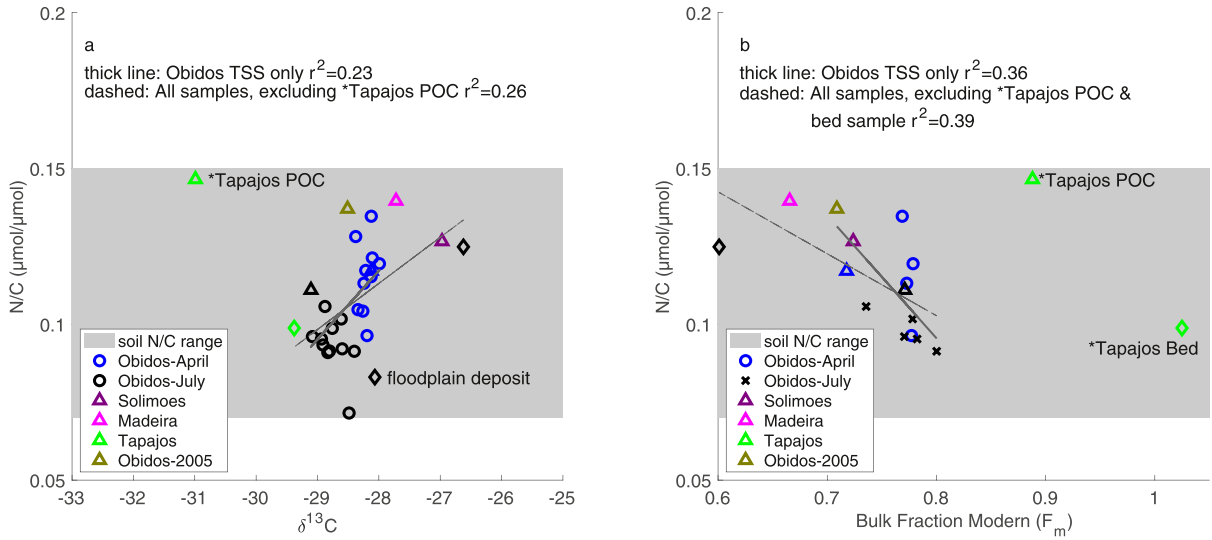

Figure 8. Bulk N/C ratios (the inverse of C/N) as a function of (a) $\delta^{13}C$ (‰) and (b) fraction modern (F_m) in samples collected in June 2005, April 2014, and July 2014. In the legend, colors are specific to location and/or time, while the symbols refer to sample type (circles for depth-specific samples, triangles for surface samples, and diamonds for bed/floodplain samples). The shaded box represents the range of known N/C ratios for soil and soil microbial biomass in the Amazon River Basin (Quesada et al., 2010, 2020; Xu et al., 2013).

less variable F_m and grain size profiles in April (Figure 2). This understanding is consistent with earlier Amazon River Basin studies that typically divided riverine POC between an older <63 µm "fine" fraction and a fresher >63 µm "coarse" fraction (Aufdenkampe et al., 2007; Hedges et al., 1986, 1994, 2000; Richey et al., 1990). But notably, we are able to report complementary results by pooling all suspended sediment data into one size-fraction (>0.2 µm), rather than into discrete size classes, assuming that organic matter degradation stages are more likely to partition along a continuum of grain sizes.

Returning to the question of sampling methodology, these bulk POC and *n*-alkane profiles suggest that even though depth-specific sampling may be necessary to accurately calculate export fluxes across the mainstem (Section 4.1), single measurements may be sufficient to understand POC composition. At worst, a single POC measurement at the surface or at a midpoint depth, rather than several throughout the cross-section, might under-sample the coarse and fresh organic matter pool that comprises the deeper and more heterogeneous source of POC in the mainstem. Thus, when comparing compositional measurements across studies, differences in sampling depth are likely less important than differences in sampling methodologies like pore size or, potentially, time of year.

4.3. Differentiating Soil Organic Matter Sources to Riverine POC

The small variations in POC composition that exist across depth profiles of the Amazon River mainstem (Section 4.2) and between the two sampling seasons do create an opportunity to explore the different processes that mobilize organic carbon in the Amazon River Basin. In addition to shifts in C/N ratio, F_m, and *n*-alkane composition within depth profiles, lower average M C/N ratios of 8.7 ± 0.89 in April compared to 10.8 ± 1.2 in July ($p < 0.05$, Student's *t*-test) in depth-specific samples, as well as significantly higher (more positive) bulk $\delta^{13}C$ values in April (−28.2 ± 0.1‰) than in July (−28.8 ± 0.2‰), suggest a shift in organic matter source between river stages.

Importantly, the abundances of *n*-alkanes and fatty acids measured in suspended sediment samples from various depths at Óbidos underscore the influence of terrestrial vegetation in riverine POC within the mainstem. Odd-over-even predominance of the higher chain length *n*-alkanes (C_{25}–C_{35}), a stronger even-over-odd predominance of the higher chain length fatty acids (C_{24}–C_{34}), and high ACL values of each compound class reflect input from land plants (Figures 4c, 5, and 6d) (Cranwell, 1982). Stable carbon isotope values for the long-chain *n*-alkanes and fatty acids are within the range of previous values measured in long-chain *n*-alkanes and fatty acids across the Amazon River Basin (Feakins et al., 2018; Häggi et al., 2016) (Tables S1 and S2, Figures 4b, 6a–6c). These isotope values are similar to the bulk leaf $\delta^{13}C$ of woody C3 plants from *terra firme* forests

(average = −32.3‰), and roughly 4‰ more depleted than C3 leaf samples from the savannah region (average = −29.0‰) (Ometto et al., 2006; Powell et al., 2012; Sanaiotti et al., 2002). Notably, these offsets are smaller than previously published offsets (e.g., ∼5.9‰ difference between *n*-alkanes and bulk C3 leaves) (Collister et al., 1994), suggesting additional sources of ^{13}C-enriched *n*-alkanes.

The small presence of high elevation plants from the Andes and C4 plants from southern regions of the Amazon River floodplain could contribute ^{13}C-enriched *n*-alkanes in the mainstem (Feakins et al., 2018; Feng et al., 2016; Martinelli et al., 1994; Powell et al., 2012; Wu et al., 2017). Another reason that compound-specific δ^{13}C values are more ^{13}C-enriched than expected for fresh vegetation is that the majority of vegetation-derived POC in the Amazon River Basin enters the river via the soil organic matter reservoir, which bears a strong degraded vegetation signature (Feakins et al., 2018; Hedges et al., 1986). Indeed, long-chain ($C_{24\text{-}32}$) fatty acids from Óbidos in 2005 exhibited a fraction modern value of 0.83, corresponding to 1,530 ^{14}C years (Eglinton et al., 2021), implying that a significant fraction of the organic matter derived from vegetation in the mainstem POC is likely pre-aged. If these *n*-alkanes came from atmospheric CO_2 that was fixed centuries ago, the Suess Effect (Ehleringer et al., 2000; Feakins et al., 2018) could have a compound effect in raising the δ^{13}C value of older *n*-alkanes relative to modern vegetation.

Adding to the argument that riverine POC is largely soil derived and pre-aged, the bulk C/N and δ^{13}C values measured for POC throughout the mainstem at Óbidos are within the range of values observed for soils across the drainage basin (Table 3, Figure 2) (Quesada et al., 2010, 2020; Sanaiotti et al., 2002). Mainstem C/N ratios, in particular, closely approximate values observed in tropical soil microbial biomass (∼9) (Xu et al., 2013), suggesting that bacterial communities must contribute an important fraction of the organic matter in these exported soil pools. Figure 8a illustrates a weak but positive correlation between bulk N/C (the inverse of C/N) and δ^{13}C values measured in suspended sediments at Óbidos, highlighting a mixing relationship between a fresher, low N/C (high C/N), and ^{13}C-depleted end-member and a more degraded, high N/C (low C/N), and ^{13}C-enriched end-member (r^2 = 0.23). This mixing relationship is slightly stronger in July samples only (r^2 = 0.34), and when including bedload, floodplain deposit and upstream tributary samples (r^2 = 0.26). Figure 8b illustrates a complementary negative relationship between bulk N/C (the inverse of C/N) and F_m values in the same samples (r^2 = 0.36–0.39), supporting the perspective that these low N/C (high C/N) samples are indeed younger in age (higher F_m), while the high N/C (low C/N) samples are older (lower F_m).

Two non-mutually exclusive hypotheses could account for these distinct soil-derived end-members exported by the Amazon River mainstem: (a) the mixing of several soil sources from different landscapes that bear distinct δ^{13}C signatures and degradation histories, and (b) the mixing of soils from different depth horizons throughout the drainage basin. The first hypothesis makes sense considering that, while the majority of the surface area covering Amazônia is dominated by ^{13}C-depleted C3 landscapes in the low-lying floodplain, there are sources of more ^{13}C-enriched POC from C4 grassland ecosystems and higher altitude Andean landscapes. The soil POC exported by higher elevation landscapes into the Madeira and Solimões Rivers are ^{13}C-enriched relative to floodplain POC because of altitude effects (Aufdenkampe et al., 2007; Feakins et al., 2018; Wu et al., 2017) and the flushing of petrogenic organic carbon (Bouchez et al., 2014).

To return to seasonality, this mixing of geographically and isotopically diverse landscapes, both soil-derived and petrogenic, would provide one explanation for the slight differences in the bulk POC composition observed at Óbidos between sampling months. The more ^{13}C-depleted/N-depleted and younger (lower F_m) bulk values in July (Table 3) are consistent with increased drainage of the adjacent floodplain and várzea lakes, where soils are replete with the residual organic carbon of C_3 plants (Feakins et al., 2018; Moreira-Turcq et al., 2013; Quay et al., 1992). Floodplain lakes, in particular, can entrap POC and resupply POC to the mainstem during receding water levels (Park & Latrubesse, 2019). Past measurements of CO_2 evasion fluxes further suggest that such flooded landscapes export relatively fresh organic matter (Abril et al., 2014). Thus, this enhanced exchange between floodplain and riverine POC explains how the C/N ratio of suspended POC in July is closer in composition to that of the N-depleted floodplain deposit sample, and how coarser, less degraded particles from floodplain lakes could end up accumulating in the deeper sections of the river during this season (Figure 2).

By contrast, the more ^{13}C-enriched/N-enriched and older (lower F_m) distribution of data from April 2014 implies that the mainstem during rising waters is influenced by a greater proportion of POC from several upstream tributaries. POC in this sampling month is compositionally more similar to the signature of the Solimões and Madeira River samples (Table 3, Figure 8). Indeed, data from the Agência Nacional de Águas show that Solimões

River discharge rose from April to May 2014, while Madeira River discharge peaked in March–April 2014 and decreased thereafter. In addition, increased incidence of landslides in the Andes during the months leading up to April would increase the input of high altitude ^{13}C-enriched POC from these tributaries (Clark et al., 2013), and the supply of old petrogenic organic carbon (Bouchez et al., 2014) to Óbidos. The preferential transport of the more degraded pools of this Andean soil source to Óbidos would explain both the more degraded and ^{13}C-enriched signatures of POC observed in April as well.

The second hypothesis could also explain the partitioning of POC in the mainstem because soil organic matter across the Amazon River Basin typically gets more ^{13}C-enriched with depth within the first ~2 m below the surface, a result of microbial degradation and the Suess Effect (Ehleringer et al., 2000; Ometto et al., 2006; Sanaiotti et al., 2002; Wu et al., 2019). Feakins et al. (2018) also found that the δ^{13}C values of *n*-alkanes in soils from the Madre de Dios River catchment area in the Andes were more ^{13}C-enriched due to flushing from deeper, older soil layers. This second hypothesis does not exclude the importance of riverine POC sources from different landscapes (i.e., our first mechanism, described above). But, similar to hypothesis one, it does explain the temporal shifts in bulk δ^{13}C and C/N values of POC at Óbidos, particularly the greater input of ^{13}C-depleted, higher C/N soil POC in July, as falling river waters draw more carbon from the superficial layers of the floodplain (Bouchez et al., 2014). Again, input of this fresher organic matter to the river in July is consistent with accumulation of higher F_m POC from coarser and less degraded vegetation debris in the deeper sections of the river (Figure 2).

4.4. Radiocarbon Ages in the Tapajós River

While floodplain lakes surrounding the mainstem have been observed to be sites of high phytoplankton and macrophyte growth, in situ primary production is not a significant component of riverine organic matter at Óbidos (Moreira-Turcq et al., 2013; Saliot et al., 2001). This is particularly clear when compared to the composition of Tapajós POC, which clearly falls off the mixing line in Figure 8a, with its high N/C (low C/N) and low δ^{13}C value. This observation is consistent with prior observations of Tapajós River POC composition and chlorophyll-a concentrations that imply a dominant input of in situ primary production (Martinelli et al., 1994; Mortillaro et al., 2011; Ward et al., 2015). The combination of a relatively deep euphotic zone depth (from low TSS concentrations) and slower water velocities in the Tapajós River, especially during the low water season, encourages greater growth of phytoplankton and cyanobacteria compared to the sediment-rich Amazon River (Mortillaro et al., 2011).

Far greater C_{16} and C_{18} abundances (23.2 ng/μg POC and 11.4 ng/μg POC, respectively) relative to higher chain length fatty acids, driving a lower fatty acid-based ACL value at the tributary surface (Figure 6d), also highlight the dominance of phytoplankton-derived organic matter in July 2014 (Cranwell, 1982; Mortillaro et al., 2011) (Table S2), while it is comparatively absent in fatty acid distributions from the mainstem and both the Solimões and Madeira Rivers. Interestingly, even-over-odd predominance of fatty acids in this sample suggests that vegetation still comprises a source of POC in the Tapajós River. Thus, it is possible that Tapajós River POC reflects a constantly shifting balance between terrestrial POC inputs and primary production, which could explain observations of more ^{13}C-enriched POC collected during other months of the year in this tributary (e.g., Mortillaro et al., 2011; Ward et al., 2015).

The radiocarbon ages measured in the Tapajós River samples are more perplexing. The Tapajós River bed sample exhibited a modern-aged F_m value of 1.02 (Table 3, Figure 8b), supporting the perspective that fresh organic matter is indeed a source of organic material deposited on the river bed, though its δ^{13}C and C/N signature implies a terrestrial, rather than phytoplankton-derived, source (Martinelli et al., 1994; Quesada et al., 2010) (Figure 8a). Possibly, backwashing of the Amazon River mainstem into the Tapajós River slows the river flow down enough to promote settling of coarse and fresh POC flushed in from the floodplain, complicating the inputs of river carbon to the Tapajós bedload (Fricke et al., 2017). Preferential respiration of autochthonous organic matter and burial of terrestrial POC may also contribute to the terrestrial signature of the Tapajós river bed (Bertassoli Jr et al., 2017). More importantly, the suspended POC in the Tapajós River is not modern, exhibiting a surprisingly low $F_m < 0.9$ (Table 3, Figure 8b). Assuming in situ fixation of DIC with a modern radiocarbon age, an age which is empirically unknown for the Tapajós River but observed elsewhere across the floodplain (Mayorga et al., 2005), one would have expected a Tapajós POC F_m value >1, similar to the bed sample. More seasonal measurements of Tapajós

POC, and further analyses of the radiocarbon age distribution of bulk POC using temperature-controlled ramped pyrolysis/oxidation analysis (Hage et al., 2020; Rosenheim & Galy, 2012) could provide further insight toward the isotopically distinct POC exported by the Tapajós River.

5. Conclusions

As the world's largest river by discharge and drainage basin, the Amazon River mainstem transports over 10 Tg of particulate organic carbon (POC) per year, representing the fraction of organic carbon export from this river basin with the highest likelihood of sequestration in Atlantic Ocean sediments. Building upon decades of prior research, our bulk and compound-specific analyses of POC from two Óbidos surveys (2005 and 2014) highlight that the majority of these particles are small-sized, well mixed in the water column, and soil-derived. This quantity of soil-derived POC exported from the Amazon River Basin alone comprises 1% of the magnitude of the increase in global riverine organic carbon export to the ocean during the Industrial Revolution from soil mobilization, 1 ± 0.5 Gt carbon per year (Friedlingstein et al., 2019; Regnier et al., 2013).

At the same time, a smaller but non-negligible fraction of riverine particles that are larger in size are of relatively fresh origin, deriving from vegetation debris, and tend to accumulate in deeper sections of the river. The fact that our bed load measurements are so carbon-poor and old, compared to the suspended sediments, implies that this less degraded carbon pool is not deposited on the river bed and may indeed be exported to the Atlantic Ocean too. Without further (including depth-specific) measurements downstream, it is unclear how the proportions of older and younger POC change downstream, especially with input of POC from other tributaries, such as the Tapajós River, which bears a stronger aquatic production signal. Particle input from the Xingu and Tocantins Rivers downstream can alter the composition of POC that is ultimately exported to the Atlantic Ocean as well (Ward et al., 2015).

Methodologically, our approach to sampling suspended sediments from several profiles of the Amazon River cross-section shows that depth-related differences in total POC concentration follow trends expected from vertical hydrodynamic sorting, supporting the application of the depth-specific sampling approach to calculate export fluxes in large rivers in the Amazon River Basin. However, because vertical differences in organic matter composition are comparatively small, the depth-specific sampling approach is perhaps not essential for tracing the sources of POC exported by the Amazon River. Given the large seasonal variations in Amazon River discharge, it is possible that this conclusion is not applicable for suspended sediments from other stages of the hydrological cycle before and after the high/peak flow months, which we did not sample. Undoubtedly, the mobilization of coarse and fresh organic debris into the river can vary throughout the year with different seasonal drainage patterns over the river basin. For future studies in the mainstem and surrounding tributaries, one potential approach that might balance accuracy and analytical effort would prioritize cross-sectional analyses of POC composition when z_R values are greater than a certain threshold (e.g., $z_R > 0.25$). This approach would still require depth-specific sampling to calculate flux and derive a z_R value during each field assay, but it would limit further compositional measurements of these depth-specific samples. This "middle ground" approach could be a valuable in other large drainage basins and deep, wide rivers that exhibit hydrodynamic sorting and a seasonality like the Amazon River.

Data Availability Statement

All discrete sample data for this research are included and tabulated in the current paper and its supplementary information files, as well as in Bouchez, Métivier, et al. (2011) and Bouchez et al. (2014). These sample data, including raw water velocity data sets obtained from the Acoustic Doppler Current Profiler, are further located in an open access (Creative Commons Attribution 4.0 International) repository on Zenodo (Rosengard, 2023). Readers may access this repository by navigating to the following DOI address in their Internet browser: https://doi.org/10.5281/zenodo.8392815.

Acknowledgments

Sarah Rosengard, Rob Spencer, and Valier Galy wrote the manuscript, with input from the other co-authors and several useful comments from two anonymous reviewers. Sarah Rosengard, Robert G.M. Spencer, Valier Galy, Jose Mauro S. Moura, and Andrew Steen participated in the field work in 2014. Sarah Rosengard, Carl Johnson, Ann McNichol, and Andrew Steen analyzed the field samples. The research was funded by the Woodwell Climate Research Center, the Woods Hole Oceanographic Institution Coastal Ocean Institute grant, the National Science Foundation Graduate Research Fellowship Program, and a U.S. National Science Foundation Grant to Valier Galy (OCE-1851309). We extend our special gratitude to Rardiles Branches, Miyuki Mitsuya, Polyana Valente, and Gabriela Vidal, students from the Universidade Federal do Oeste do Pará; our field work on the Rio Amazonas and Rio Tapajós could not have been done without them.

References

Abril, G., Martinez, J.-M., Artigas, L. F., Moreira-Turcq, P., Benedetti, M. F., Vidal, L., et al. (2014). Amazon River carbon dioxide outgassing fuelled by wetlands. *Nature*, *505*(7483), 395–398. https://doi.org/10.1038/nature12797

Amon, R. M. W., & Benner, R. (1996). Bacterial utilization of different size classes of dissolved organic matter. *Limnology & Oceanography*, *41*(1), 41–51. https://doi.org/10.4319/lo.1996.41.1.0041

Aufdenkampe, A. K., Mayorga, E., Hedges, J. I., Llerena, C., Quay, P. D., Gudeman, J., et al. (2007). Organic matter in the Peruvian headwaters of the Amazon: Compositional evolution from the Andes to the lowland Amazon mainstem. *Organic Geochemistry*, *38*(3), 337–364. https://doi.org/10.1016/j.orggeochem.2006.06.003

Baltar, F. (2018). Watch out for the "living dead": Cell-free enzymes and their fate. *Frontiers in Microbiology*, *8*, 2438. https://doi.org/10.3389/fmicb.2017.02438

Bertassoli Jr, D. J., Sawakuchi, A. O., Sawakuchi, H. O., Pupim, F. N., Hartmann, G. A., McGlue, M. M., et al. (2017). The fate of carbon in sediments of the Xingu and Tapajós clearwater rivers, Eastern Amazon. *Frontiers in Marine Science*, *4*, 44. https://doi.org/10.3389/fmars.2017.00044

Bouchez, J., Beyssac, O., Galy, V., Gaillardet, J., France-Lanord, C., Maurice, L., & Moreira-Turcq, P. (2010). Oxidation of petrogenic organic carbon in the Amazon floodplain as a source of atmospheric CO_2. *Geology*, *38*(3), 255–258. https://doi.org/10.1130/g30608.1

Bouchez, J., Gaillardet, J., France-Lanord, C., Maurice, L., & Dutra-Maia, P. (2011). Grain size control of river suspended sediment geochemistry: Clues from Amazon River depth profiles. *Geochemistry, Geophysics, Geosystems*, *12*(3), Q03008. https://doi.org/10.1029/2010gc003380

Bouchez, J., Galy, V., Hilton, R. G., Gaillardet, J., Moreira-Turcq, P., Pérez, M. A., et al. (2014). Source, transport and fluxes of Amazon River particulate organic carbon: Insights from river sediment depth-profiles. *Geochimica et Cosmochimica Acta*, *133*, 280–298. https://doi.org/10.1016/j.gca.2014.02.032

Bouchez, J., Métivier, F., Lupker, M., Maurice, L., Perez, M., Gaillardet, J., & France-Lanord, C. (2011). Prediction of depth-integrated fluxes of suspended sediment in the Amazon River: Particle aggregation as a complicating factor. *Hydrological Processes*, *25*(5), 778–794. https://doi.org/10.1002/hyp.7868

Chen, C. (1989). Power law of flow resistance in open channels, Manning's formula revisited.

Clark, K. E., Hilton, R. G., West, A. J., Malhi, Y., Gröcke, D. R., Bryant, C. L., et al. (2013). New views on "old" carbon in the Amazon River: Insight from the source of organic carbon eroded from the Peruvian Andes. *Geochemistry, Geophysics, Geosystems*, *14*(5), 1644–1659. https://doi.org/10.1002/ggge.20122

Collister, J. W., Rieley, G., Stern, B., Eglinton, G., & Fry, B. (1994). Compound-specific $\delta^{13}C$ analyses of leaf lipids from plants with differing carbon dioxide metabolisms. *Organic Geochemistry*, *21*(6–7), 619–627. https://doi.org/10.1016/0146-6380(94)90008-6

Cranwell, P. A. (1982). Lipids of aquatic sediments and sedimenting particulates. *Progress in Lipid Research*, *21*(4), 271–308. https://doi.org/10.1016/0163-7827(82)90012-1

Curtis, W. F., Meade, R. H., Nordin, C. F., Jr., Price, N. B., & Sholkovitz, E. R. (1979). Non-uniform vertical distribution of fine sediment in the Amazon River. *Nature*, *280*(5721), 381–383. https://doi.org/10.1038/280381a0

Dai, A., & Trenberth, K. E. (2002). Estimates of freshwater discharge from continents: Latitudinal and seasonal variations. *Journal of Hydrometeorology*, *3*(6), 660–687. https://doi.org/10.1175/1525-7541(2002)003<0660:eofdfc>2.0.co;2

Eglinton, G., & Hamilton, R. J. (1963). The distribution of alkanes. *Chemical Plant Taxonomy*, *187*, 217.

Eglinton, T. I., Galy, V. V., Hemingway, J. D., Feng, X., Bao, H., Blattmann, T. M., et al. (2021). Climate control on terrestrial biospheric carbon turnover. *Proceedings of the National Academy of Sciences of the United States of America*, *118*(8), e2011585118. https://doi.org/10.1073/pnas.2011585118

Ehleringer, J. R., Buchmann, N., & Flanagan, L. B. (2000). Carbon isotope ratios in belowground carbon cycle processes. *Ecological Applications*, *10*(2), 412–422. https://doi.org/10.2307/2641103

Feakins, S. J., Wu, M. S., Ponton, C., Galy, V., & West, A. J. (2018). Dual isotope evidence for sedimentary integration of plant wax biomarkers across an Andes-Amazon elevation transect. *Geochimica et Cosmochimica Acta*, *242*, 64–81. https://doi.org/10.1016/j.gca.2018.09.007

Feng, X., Feakins, S. J., Liu, Z., Ponton, C., Wang, R. Z., Karkabi, E., et al. (2016). Source to sink: Evolution of lignin composition in the Madre de Dios River system with connection to the Amazon basin and offshore. *Journal of Geophysical Research: Biogeosciences*, *121*(5), 1316–1338. https://doi.org/10.1002/2016jg003323

Fricke, A. T., Nittrouer, C. A., Ogston, A. S., Nowacki, D. J., Asp, N. E., Souza Filho, P. W. M., et al. (2017). River tributaries as sediment sinks: Processes operating where the Tapajós and Xingu rivers meet the Amazon tidal river. *Sedimentology*, *64*(6), 1731–1753. https://doi.org/10.1111/sed.12372

Friedlingstein, P., Jones, M. W., O'sullivan, M., Andrew, R. M., Hauck, J., Peters, G. P., et al. (2019). Global carbon budget 2019. *Earth System Science Data*, *11*(4), 1783–1838. https://doi.org/10.5194/essd-11-1783-2019

Galy, V., Beyssac, O., France-Lanord, C., & Eglinton, T. (2008). Recycling of graphite during Himalayan erosion: A geological stabilization of carbon in the crust. *Science*, *322*(5903), 943–945. https://doi.org/10.1126/science.1161408

Galy, V., Peucker-Ehrenbrink, B., & Eglinton, T. (2015). Global carbon export from the terrestrial biosphere controlled by erosion. *Nature*, *521*(7551), 204–207. https://doi.org/10.1038/nature14400

Guyot, J. L., Fillzola, N., Quintanilla, J., & Cortez, J. (1996). *Dissolved solids and suspended sediment yields in the Rio Madeira basin, from the Bolivian Andes to the Amazon* (pp. 55–64). IAHS Publication.

Hage, S., Galy, V. V., Cartigny, M. J. B., Acikalin, S., Clare, M. A., Gröcke, D. R., et al. (2020). Efficient preservation of young terrestrial organic carbon in sandy turbidity-current deposits. *Geology*, *48*(9), 882–887. https://doi.org/10.1130/g47320.1

Häggi, C., Sawakuchi, A. O., Chiessi, C. M., Mulitza, S., Mollenhauer, G., Sawakuchi, H. O., et al. (2016). Origin, transport and deposition of leaf-wax biomarkers in the Amazon Basin and the adjacent Atlantic. *Geochimica et Cosmochimica Acta*, *192*, 149–165. https://doi.org/10.1016/j.gca.2016.07.002

Hedges, J. I., Clark, W. A., Quay, P. D., Richey, J. E., Devol, A. H., & Santos, M. (1986). Compositions and fluxes of particulate organic material in the Amazon River 1. *Limnology & Oceanography*, *31*(4), 717–738. https://doi.org/10.4319/lo.1986.31.4.0717

Hedges, J. I., Cowie, G. L., Richey, J. E., Quay, P. D., Benner, R., Strom, M., & Forsberg, B. R. (1994). Origins and processing of organic matter in the Amazon River as indicated by carbohydrates and amino acids. *Limnology & Oceanography*, *39*(4), 743–761. https://doi.org/10.4319/lo.1994.39.4.0743

Hedges, J. I., Mayorga, E., Tsamakis, E., McClain, M. E., Aufdenkampe, A., Quay, P., et al. (2000). Organic matter in Bolivian tributaries of the Amazon River: A comparison to the lower mainstream. *Limnology & Oceanography*, *45*(7), 1449–1466. https://doi.org/10.4319/lo.2000.45.7.1449

Hemingway, J. D., Schefuß, E., Dinga, B. J., Pryer, H., & Galy, V. V. (2016). Multiple plant-wax compounds record differential sources and ecosystem structure in large river catchments. *Geochimica et Cosmochimica Acta*, *184*, 20–40. https://doi.org/10.1016/j.gca.2016.04.003

Kim, J.-H., Zell, C., Moreira-Turcq, P., Pérez, M. A. P., Abril, G., Mortillaro, J.-M., et al. (2012). Tracing soil organic carbon in the lower Amazon River and its tributaries using GDGT distributions and bulk organic matter properties. *Geochimica et Cosmochimica Acta*, *90*, 163–180. https://doi.org/10.1016/j.gca.2012.05.014

Kosuth, P., Callede, J., Laraque, A., Filizola, N., Guyot, J. L., Seyler, P., et al. (2009). Sea-tide effects on flows in the lower reaches of the Amazon River. *Hydrological Processes: An International Journal*, *23*(22), 3141–3150. https://doi.org/10.1002/hyp.7387

Lupker, M., France-Lanord, C., Lavé, J., Bouchez, J., Galy, V., Métivier, F., et al. (2011). A Rouse-based method to integrate the chemical composition of river sediments: Application to the Ganga basin. *Journal of Geophysical Research*, *116*(F4), F04012. https://doi.org/10.1029/2010jf001947

Martinelli, L. A., Victoria, R. L., Forsberg, B. R., & Richey, J. E. (1994). Isotopic composition of major carbon reservoirs in the Amazon floodplain. *International Journal of Ecology & Environmental Sciences*, *20*(1), 31–46.

Mayorga, E., Aufdenkampe, A. K., Masiello, C. A., Krusche, A. V., Hedges, J. I., Quay, P. D., et al. (2005). Young organic matter as a source of carbon dioxide outgassing from Amazonian rivers. *Nature*, *436*(7050), 538–541. https://doi.org/10.1038/nature03880

McNichol, A. P., Gagnon, A. R., Jones, G. A., & Osborne, E. A. (1992). Illumination of a black box: Analysis of gas composition during graphite target preparation. *Radiocarbon*, *34*(3), 321–329. https://doi.org/10.1017/s0033822200063499

McNichol, A. P., Gagnon, A. R., Osborne, E. A., Hutton, D. L., Von Reden, K. F., & Schneider, R. J. (1995). Improvements in procedural blanks at NOSAMS: Reflections of improvements in sample preparation and accelerator operation. *Radiocarbon*, *37*(2), 683–691. https://doi.org/10.1017/s0033822200031209

Moreira-Turcq, P., Bonnet, M., Amorim, M., Bernardes, M., Lagane, C., Maurice, L., et al. (2013). Seasonal variability in concentration, composition, age, and fluxes of particulate organic carbon exchanged between the floodplain and Amazon River. *Global Biogeochemical Cycles*, *27*(1), 119–130. https://doi.org/10.1002/gbc.20022

Moreira-Turcq, P., Seyler, P., Guyot, J. L., & Etcheber, H. (2003). Exportation of organic carbon from the Amazon River and its main tributaries. *Hydrological Processes*, *17*(7), 1329–1344. https://doi.org/10.1002/hyp.1287

Mortillaro, J.-M., Abril, G., Moreira-Turcq, P., Sobrinho, R. L., Perez, M., & Meziane, T. (2011). Fatty acid and stable isotope ($\delta^{13}C$, $\delta^{15}N$) signatures of particulate organic matter in the lower Amazon River: Seasonal contrasts and connectivity between floodplain lakes and the mainstem. *Organic Geochemistry*, *42*(10), 1159–1168. https://doi.org/10.1016/j.orggeochem.2011.08.011

Mueller, D. S., Wagner, C. R., Rehmel, M. S., Oberg, K. A., & Rainville, F. (2009). *Measuring discharge with acoustic Doppler current profilers from a moving boat*. US Department of the Interior, US Geological Survey Reston.

Mullen, L., Boerrigter, K., Ferriero, N., Rosalsky, J., van Barrett, A. B., Murray, P. J., & Steen, A. D. (2018). Potential activities of freshwater exo- and endo-acting extracellular peptidases in East Tennessee and the Pocono Mountains. *Frontiers in Microbiology*, *9*, 368. https://doi.org/10.3389/fmicb.2018.00368

Ometto, J. P. H. B., Ehleringer, J. R., Domingues, T. F., Berry, J. A., Ishida, F. Y., Mazzi, E., et al. (2006). The stable carbon and nitrogen isotopic composition of vegetation in tropical forests of the Amazon Basin, Brazil. *Biogeochemistry*, *79*(1–2), 251–274. https://doi.org/10.1007/978-1-4020-5517-1_12

Park, E., & Latrubesse, E. M. (2019). A geomorphological assessment of wash-load sediment fluxes and floodplain sediment sinks along the lower Amazon River. *Geology*, *47*(5), 403–406. https://doi.org/10.1130/g45769.1

Powell, R. L., Yoo, E.-H., & Still, C. J. (2012). Vegetation and soil carbon-13 isoscapes for South America: Integrating remote sensing and ecosystem isotope measurements. *Ecosphere*, *3*(11), 1–25. https://doi.org/10.1890/es12-00162.1

Quay, P. D., Wilbur, D. 0, Richey, J. E., Hedges, J. I., Devol, A. H., & Victoria, R. (1992). Carbon cycling in the Amazon River: Implications from the ^{13}C compositions of particles and solutes. *Limnology & Oceanography*, *37*(4), 857–871. https://doi.org/10.4319/lo.1992.37.4.0857

Quesada, C. A., Lloyd, J., Schwarz, M., Patiño, S., Baker, T. R., Czimczik, C., et al. (2010). Variations in chemical and physical properties of Amazon forest soils in relation to their genesis. *Biogeosciences*, *7*(5), 1515–1541. https://doi.org/10.5194/bg-7-1515-2010

Quesada, C. A., Paz, C., Oblitas Mendoza, E., Phillips, O. L., Saiz, G., & Lloyd, J. (2020). Variations in soil chemical and physical properties explain basin-wide Amazon forest soil carbon concentrations. *Soil*, *6*(1), 53–88. https://doi.org/10.5194/soil-6-53-2020

Regnier, P., Friedlingstein, P., Ciais, P., Mackenzie, F. T., Gruber, N., Janssens, I. A., et al. (2013). Anthropogenic perturbation of the carbon fluxes from land to ocean. *Nature Geoscience*, *6*(8), 597–607. https://doi.org/10.1038/ngeo1830

Richey, J. E., Hedges, J. I., Devol, A. H., Quay, P. D., Victoria, R., Martinelli, L., & Forsberg, B. R. (1990). Biogeochemistry of carbon in the Amazon River. *Limnology & Oceanography*, *35*(2), 352–371. https://doi.org/10.4319/lo.1990.35.2.0352

Richey, J. E., Meade, R. H., Salati, E., Devol, A. H., Nordin Jr, C. F., & Santos, U. D. (1986). Water discharge and suspended sediment concentrations in the Amazon River: 1982–1984. *Water Resources Research*, *22*(5), 756–764. https://doi.org/10.1029/wr022i005p00756

Richey, J. E., Melack, J. M., Aufdenkampe, A. K., Ballester, V. M., & Hess, L. L. (2002). Outgassing from Amazonian rivers and wetlands as a large tropical source of atmospheric CO_2. *Nature*, *416*(6881), 617–620. https://doi.org/10.1038/416617a

Rosengard, S. (2023). Obidos 2014—Part 1. https://doi.org/10.5281/ZENODO.8392815

Rosenheim, B. E., & Galy, V. (2012). Direct measurement of riverine particulate organic carbon age structure. *Geophysical Research Letters*, *39*(19), L19703. https://doi.org/10.1029/2012gl052883

Rouse, H. (1950). *Engineering hydraulics* (p. 414). John Wiley and Sons. Inc.

Saliot, A., Mejanelle, L., Scribe, P., Fillaux, J., Pepe, C., Jabaud, A., & Dagaut, J. (2001). Particulate organic carbon, sterols, fatty acids and pigments in the Amazon River system. *Biogeochemistry*, *53*(1), 79–103. https://doi.org/10.1023/a:1010754022594

Sanaiotti, T. M., Martinelli, L. A., Victória, R. L., Trumbore, S. E., & de Camargo, P. B. (2002). Past vegetation changes in Amazon Savannas determined using carbon isotopes of soil organic matter 1. *Biotropica*, *34*(1), 2–16. https://doi.org/10.1646/0006-3606(2002)034[0002:pvcias]2.0.co;2

Satinsky, B. M., Crump, B. C., Smith, C. B., Sharma, S., Zielinski, B. L., Doherty, M., et al. (2014). Microspatial gene expression patterns in the Amazon River Plume. *Proceedings of the National Academy of Sciences of the United States of America*, *111*(30), 11085–11090. https://doi.org/10.1073/pnas.1402782111

Sun, S., Schefuß, E., Mulitza, S., Chiessi, C. M., Sawakuchi, A. O., Zabel, M., et al. (2017). Origin and processing of terrestrial organic carbon in the Amazon system: Lignin phenols in river, shelf, and fan sediments. *Biogeosciences*, *14*(9), 2495–2512. https://doi.org/10.5194/bg-14-2495-2017

Volkman, J. K., Holdsworth, D. G., Neill, G. P., & Bavor Jr, H. J. (1992). Identification of natural, anthropogenic and petroleum hydrocarbons in aquatic sediments. *Science of the Total Environment*, *112*(2–3), 203–219. https://doi.org/10.1016/0048-9697(92)90188-x

Ward, N. D., Keil, R. G., Medeiros, P. M., Brito, D. C., Cunha, A. C., Dittmar, T., et al. (2013). Degradation of terrestrially derived macromolecules in the Amazon River. *Nature Geoscience*, *6*(7), 530–533. https://doi.org/10.1038/ngeo1817

Ward, N. D., Krusche, A. V., Sawakuchi, H. O., Brito, D. C., Cunha, A. C., Moura, J. M. S., et al. (2015). The compositional evolution of dissolved and particulate organic matter along the lower Amazon River—Óbidos to the ocean. *Marine Chemistry*, *177*, 244–256. https://doi.org/10.1016/j.marchem.2015.06.013

Ward, N. D., Sawakuchi, H. O., Neu, V., Less, D. F. S., Valerio, A. M., Cunha, A. C., et al. (2018). Velocity-amplified microbial respiration rates in the lower Amazon River. *Limnology and Oceanography Letters*, *3*(3), 265–274. https://doi.org/10.1002/lol2.10062

Ward, N. D., Sawakuchi, H. O., Richey, J. E., Keil, R. G., & Bianchi, T. S. (2019). Enhanced aquatic respiration associated with mixing of clearwater tributary and turbid Amazon river waters. *Frontiers in Earth Science*, *7*, 101. https://doi.org/10.3389/feart.2019.00101

Whiteside, J. H., Olsen, P. E., Eglinton, T. I., Cornet, B., McDonald, N. G., & Huber, P. (2011). Pangean great lake paleoecology on the cusp of the end-Triassic extinction. *Palaeogeography, Palaeoclimatology, Palaeoecology*, *301*(1–4), 1–17. https://doi.org/10.1016/j.palaeo.2010.11.025

Wu, M. S., Feakins, S. J., Martin, R. E., Shenkin, A., Bentley, L. P., Blonder, B., et al. (2017). Altitude effect on leaf wax carbon isotopic composition in humid tropical forests. *Geochimica et Cosmochimica Acta*, *206*, 1–17. https://doi.org/10.1016/j.gca.2017.02.022

Wu, M. S., West, A. J., & Feakins, S. J. (2019). Tropical soil profiles reveal the fate of plant wax biomarkers during soil storage. *Organic Geochemistry*, *128*, 1–15. https://doi.org/10.1016/j.orggeochem.2018.12.011

Xu, X., Thornton, P. E., & Post, W. M. (2013). A global analysis of soil microbial biomass carbon, nitrogen and phosphorus in terrestrial ecosystems. *Global Ecology and Biogeography*, *22*(6), 737–749. https://doi.org/10.1111/geb.12029